

RESEARCH ARTICLE

10.1002/2016JE005108

Key Points:

- Effusive volcanism in the Late Amazonian dominated volcanic activity on Olympus Mons
- Volcanotectonic activity (e.g., flank vents and graben) was largely restricted to the lower flanks of Olympus Mons
- Olympus Mons has evolved similarly to other large Martian shield volcanoes such as Ascræus Mons

Supporting Information:

- Supporting Information S1
- Data Set S1

Correspondence to:

S. I. Peters,
speter24@asu.edu

Citation:


Peters, S. I., and P. R. Christensen (2017), Flank vents and graben as indicators of Late Amazonian volcanotectonic activity on Olympus Mons, *J. Geophys. Res. Planets*, 122, doi:10.1002/2016JE005108.

Received 14 JUN 2016

Accepted 11 FEB 2017

Accepted article online 15 FEB 2017

Flank vents and graben as indicators of Late Amazonian volcanotectonic activity on Olympus Mons

S. I. Peters¹  and P. R. Christensen¹¹School of Earth and Space Exploration, Arizona State University, Tempe, Arizona, USA

Abstract Previous studies have focused on large-scale features on Olympus Mons, such as its flank terraces, the summit caldera complex, and the basal escarpment and aureole deposits. Here we identify and characterize previously unrecognized and unmapped small scale features to help further understand the volcanotectonic evolution of this enormous volcano. Using Context Camera, High Resolution Imaging Science Experiment, Thermal Emission Imaging System, High Resolution Stereo Camera Digital Terrain Model, and Mars Orbiter Laser Altimeter data, we identified and characterized the morphology and distribution of 60 flank vents and 84 grabens on Olympus Mons. We find that effusive eruptions have dominated volcanic activity on Olympus Mons in the Late Amazonian. Explosive eruptions were rare, implying volatile-poor magmas and/or a lack of magma-water interactions during the Late Amazonian. The distribution of flank vents suggests dike propagation of hundreds of kilometers and shallow magma storage. Small grabens, not previously observed in lower-resolution data, occur primarily on the lower flanks of Olympus Mons and indicate late-stage extensional tectonism. Based on superposition relationships, we have concluded two stages of development for Olympus Mons during the Late Amazonian: (1) primarily effusive resurfacing and formation of flank vents followed by (2) waning effusive volcanism and graben formation and/or reactivation. This developmental sequence resembles that proposed for Ascræus Mons and other large Martian shields, suggesting a similar geologic evolution for these volcanoes.

1. Introduction

Volcanism has played a fundamental role in creating and shaping the Martian crust [Carr, 1973; Carr *et al.*, 1977; Greeley and Spudis, 1981; Wilson and Head, 1994; Werner, 2009]. At least 60% of the planet has been resurfaced by volcanism [Greeley and Spudis, 1981]. Numerous types of landforms are observed on the Martian surface, including the massive shields of the Tharsis and Elysium provinces, the highland patera, and the young flows of Cerberus Fossae [Carr, 1973; Carr *et al.*, 1977; Greeley and Spudis, 1981; Plescia, 2004; Werner, 2009]. The trend in volcanism in Martian history has been one of decreasing spatial and temporal activity and volume [Greeley and Spudis, 1981; Werner, 2009]. Additionally, there is a complex interplay between volcanism and tectonism on Mars. For example, many grabens on Mars have been interpreted as the surface expression of dikes [Carr, 1974; Wilson and Head, 2002], and arcuate or concentric graben on the flank of Ascræus Mons (one of the Tharsis Montes) might indicate gravitational spreading or flexure of the edifice [Byrne *et al.*, 2012; Pozzobon *et al.*, 2015]. Characterizing the interplay between volcanism and tectonism for a given volcano can give a fuller understanding of that edifice's developmental history. By mapping flank vents and graben on Olympus Mons, we have further characterized Late Amazonian volcanic activity on that volcano and identified recent deformation of the shield. Our results help further characterize the state of stress on the lower flanks and the magma plumbing system of this volcano and may be applicable to other large volcanoes.

1.1. Olympus Mons

Olympus Mons, the largest known volcano in the Solar System, stands approximately 22 km above the surrounding plains and is 600 km across [Carr, 1973; Blasius and Cutts, 1981; Greeley and Spudis, 1981; Plescia, 2004; Werner, 2009]. This shield volcano is situated just northwest of the Tharsis Montes to the southwest of Alba Mons. The shield hosts a variety of complex and enormous geologic features (Figure 1). A nested caldera complex approximately 90 × 60 km in size is situated at the summit [Carr, 1973; Wood, 1984; Mouginis-Mark and Rowland, 2001; Plescia, 2004]. Most of the lava flows observed to have originated from Olympus

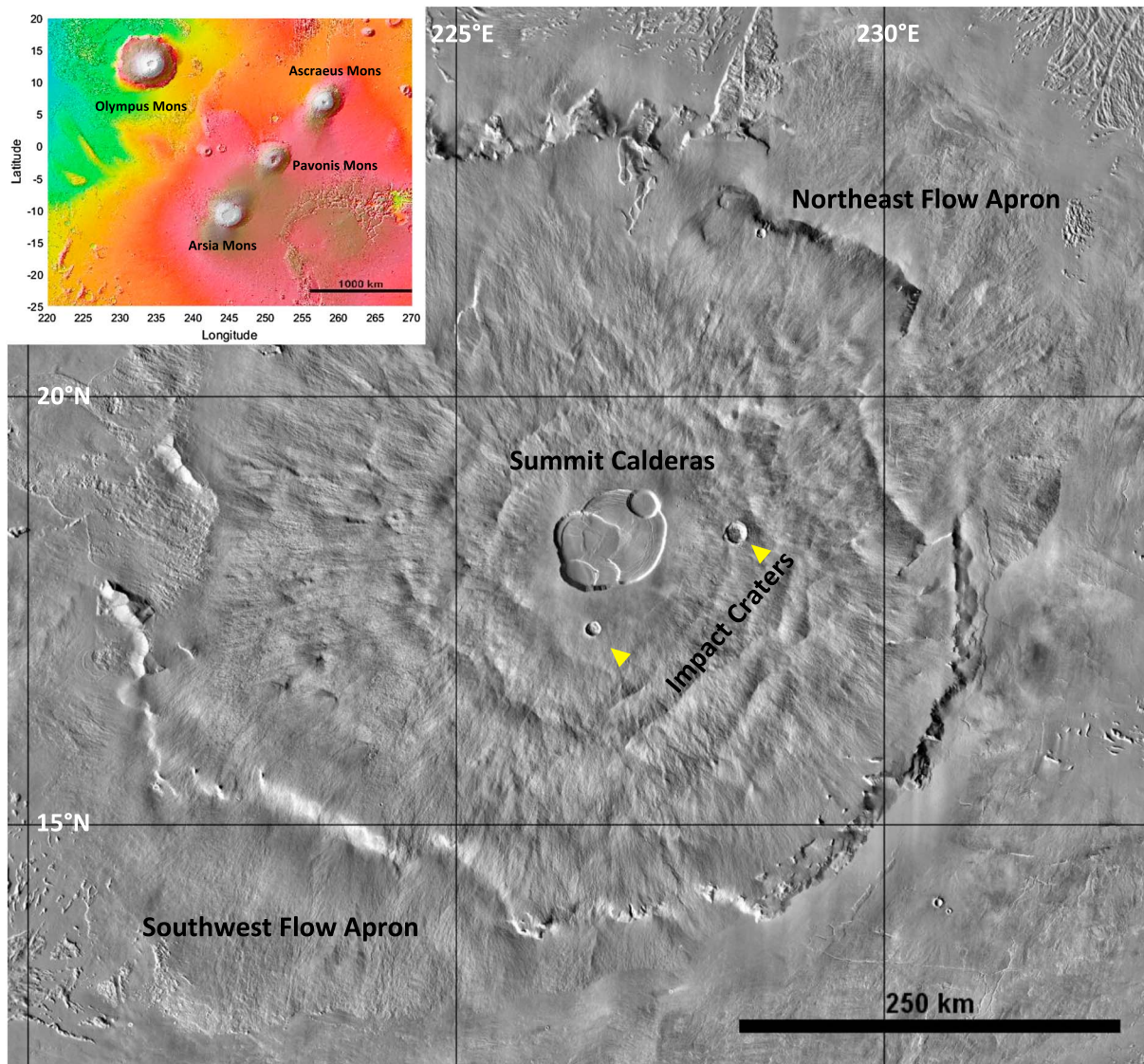


Figure 1. Inset of MOLA colorized topography of Tharsis province. Warmer colors indicate higher elevation. Cooler colors indicate lower elevation. The three smaller cones to the southeast of Olympus Mons are the Tharsis Montes. Grayscale image is THEMIS daytime infrared mosaic of Olympus Mons. Illumination is from the left. Note flow aprons mantling the basal escarpment on the northeast and southwest flanks. Rough material near edges of image is proximal aureole deposits. North is up in this and all subsequent images.

Mons are embayed by flows from Tharsis, either from the Tharsis Montes, the smaller shields, or from sources that are no longer visible [Carr *et al.*, 1977; Isherwood *et al.*, 2013; Chadwick *et al.*, 2015]. A basal escarpment ranging in height from 3 to 8 km encircles most of the shield [Carr, 1973; King and Riehle, 1974; Carr *et al.*, 1977; Tanaka, 1985; Thomas *et al.*, 1990]. To the northeast and southwest, lava flows have draped over the escarpment and obscured its topographic expression, creating two distinct aprons [Carr *et al.*, 1977; Greeley and Spudis, 1981; Neukum *et al.*, 2004]. To a lesser extent, lava has flowed off the escarpment to the south [Thomas *et al.*, 1990]. Aureole deposits, interpreted as massive landslides derived from the volcano via flank failure, extend up to 800 km away from Olympus Mons [Carr, 1973; King and Riehle, 1974; Carr *et al.*, 1977; Tanaka, 1985; Thomas *et al.*, 1990; McGovern *et al.*, 2004; Mouginiis-Mark and Christensen, 2005]. Convex-up landforms arranged in a fish scale-like imbricate pattern on the upper flanks of the shield and termed flank terraces are thought to represent thrust faulting due to flexure of the edifice [Carr *et al.*, 1977; Thomas *et al.*, 1990; McGovern and Solomon, 1993; Byrne *et al.*, 2009, 2012, 2013]. The flexure may have oversteepened the lower flanks of the volcano and so promoted slope failure [Byrne *et al.*, 2013].

Olympus Mons displays a flat summit plateau, steeper upper flanks ($\sim 5\text{--}9^\circ$), and gentler sloping lower flanks ($\sim 4^\circ$), with the steepest slopes ($\sim 25\text{--}40^\circ$) restricted to the basal escarpment [King and Riehle, 1974; Blasius and Cutts, 1981; Plescia, 2004; Byrne et al., 2013]. The physical volcanological landforms on the flanks of Olympus Mons render it morphologically similar to the Hawaiian volcanic shields, and so a basaltic composition has been inferred for its erupted lavas [Carr, 1973; Wood, 1984; Hulme, 1976; Zuber and Mouginis-Mark, 1992; Bleacher et al., 2007]. Although development of the Olympus Mons edifice probably started during the early Hesperian (~ 3.6 Ga), most of the shield's surface has been dated to the Late Amazonian (< 700 Ma) [Neukum et al., 2004; Werner, 2009; Isherwood et al., 2013; Tanaka et al., 2014]. Effusive volcanic activity dominated in the Late Amazonian, as evidenced by abundant lava tubes and channels [Carr, 1973; Carr et al., 1977; Neukum et al., 2004; Bleacher et al., 2007; Werner, 2009]. Some of the youngest features on Olympus Mons include lavas on the floors of the nested calderas ($\sim 100\text{--}200$ Ma) as well as lava flows on the volcano's southwestern flanks (≤ 50 Ma) [Neukum et al., 2004; Werner, 2009; Tanaka et al., 2014]. A few locations on the shield are substantially older (~ 3.3 Ga) and likely represent earlier portions of Olympus Mons volcano [Werner, 2009]. Like many elevated regions on Mars, the volcano's flanks and summit are blanketed in 1–2 m of dust that prevents spectral analysis and obscures finer details of the topography at comparable scales [Christensen, 1986]. Despite the dust cover, small topographic features, such as flank vents and graben, can be discerned on Olympus Mons.

1.2. Flank Vents

Flank or satellite vents are a common feature on terrestrial composite volcanoes of various compositions [Nakamura, 1977; Wood, 1980; Davidson and DeSilva, 2000; Corrazato and Tibaldi, 2006]. Examples include Cerro Azul (Galapagos Islands), Mount Etna (Sicily), and Santa Clara (Pinacates Volcanic Field, Mexico) [Nakamura, 1977; Rowland, 1996; Davidson and DeSilva, 2000; Corrazato and Tibaldi, 2006]. Vents can manifest as fissures, cinder/scoria cones, lava lakes, or low shields [Greeley, 1977; Wood, 1980; Greeley, 1982; Rowland, 1996; Davidson and DeSilva, 2000; Corrazato and Tibaldi, 2006; Hauber et al., 2009; Brož and Hauber, 2012]. Vent morphology provides information on the effusion rates, eruption style, and to a lesser extent, magma volatile content [Wood, 1980; Rowland, 1996; Davidson and DeSilva, 2000; Corrazato and Tibaldi, 2006]. The spatial distribution of flank vents provides information on the stress field acting on the volcano at the time of vent formation as well as insight into the geometry of a volcano's plumbing system—specifically the likely direction and orientation of magma propagation and magma source depths [Nakamura, 1977; Bleacher et al., 2009; Hauber et al., 2009; Kervyn et al., 2009]. The relationship between flank vents and other prominent features can also be useful in efforts to reconstruct the late-stage evolutionary sequence of the volcano [Kervyn et al., 2009; Byrne et al., 2012;].

1.3. Graben

Graben—two antithetic, parallel normal faults that bound a down-dropped block, formed in response to local or far field extensional stress—is a common feature across the Tharsis volcanic province [Carr, 1974; Wilson and Head, 2002]. They cross-cut volcanic plains as well as the Tharsis Montes and extend for thousands of kilometers wrapping around Alba Mons to the north and fanning out over Daedalia Planum to the south [Carr, 1974; Wilson and Head, 2002; Byrne et al., 2012; Pozzobon et al., 2015]. Many are hypothesized to represent the surface expression of dike propagation, especially in places like Mangala Valles where lavas appear to emanate from graben [Wilson and Head, 2002]. Others, such as those observed on the Tharsis Montes, may reflect either gravitational spreading or partial collapse of the edifice or flexure of the volcano due to adjustment of the lithosphere to the load [Elsworth and Day, 1999; McGovern and Solomon, 1993; Byrne et al., 2009; Byrne et al., 2012; Byrne et al., 2013]. Smaller concentric grabens observed around the margin of volcanic edifices likely do not represent dike propagation and may be due solely to gravitational deformation of the cone [Byrne et al., 2012]. Moreover, observations of superposition relationships between graben and flank vents can be used to determine the sequence for their formation.

2. Methods

2.1. Data Sets

We used image data from the Mars Reconnaissance Orbiter (MRO) Context Camera (CTX: ~ 5 m/pixel) [Malin et al., 2007], the Mars Odyssey Thermal Emission Imaging System infrared (THEMIS IR: 100 m/pixel) [Christensen et al., 2004], and the MRO High Resolution Imaging Science Experiment (HiRISE: ~ 0.5 m/pixel)

[McEwan *et al.*, 2007] instruments. Only two flank vents and a single graben on Olympus Mons had been imaged with HiRISE data when we prepared this manuscript. For topographic and morphometric investigations, we utilized topographic data from the Mars Global Surveyor Mars Orbital Laser Altimeter (MOLA: ~463 m/pixel) [Zuber *et al.*, 1992] data set, as well as Mars Express High Resolution Stereo Camera (HRSC) digital terrain models (DTM cell size: 50 and 75 m) [Jaumann *et al.*, 2007].

2.2. Identification and Classification of Landforms

We mosaicked 159 CTX images; we used images with similar emission angles (~0–20°) where possible, although higher-emission angles were used where necessary to ensure complete coverage of the volcano. This high-resolution data set allowed for the identification and characterization of morphologic features <50 m across. After an initial survey to identify and locate flank vents, we utilized the Catalogue of Tharsis Small Volcanic Vents [Bleacher *et al.*, 2010] to identify additional possible vents on Olympus Mons. Grabens were primarily identifiable in CTX image data; we characterized their dimensions with MOLA data. Because the relief (and the width in many cases) of these features is below that which can be resolved with High Resolution Stereo Camera Digital Terrain Models (HRSC DTMs) or MOLA, depth measurements for the graben could not be obtained; the vertical resolution of the DTMs therefore could provide a maximum depth for observed graben. We performed mapping and analysis with the Java Mission-planning and Analysis for Remote Sensing (JMARS) and Environmental Systems Research Institute ArcGIS 10.3 software.

2.3. Flank Vent Volume Calculations

With HRSC DTMs, which provided partial coverage of Olympus Mons, we then determined height and volume estimates for those vents for which we had sufficiently resolved topographic data ($n = 16$). The volumes were calculated by assuming a conical shape for those landforms we interpreted as scoria cones and low shields, small shield volcanoes with slopes averaging <1–2° [Greeley, 1977; Greeley, 1982; Davidson and DeSilva, 2000; Hauber *et al.*, 2009]. Vents do not occur on the summit plateau but are instead upon the slopes (~4–25°) of the middle to lower flanks and escarpment, which causes some preferential flow of lava downhill. This effect should result in lower edifice heights than those expected on a flat surface, since some volume erupted that would have contributed to the landform's height but instead contributes to its downslope length. The formation of scoria cones in particular is not affected by slopes <9° [Brož and Hauber, 2012], although greater slopes are present on portions of the volcano's escarpment. No cones were observed on slopes $\geq 9^\circ$, so we assumed negligible error in our morphometric measurements of cones due to this effect.

2.4. Flank Vent Slope Calculations

Given DTM coverage of only 16 of the observed vents in our study, caution must be exercised in interpreting the statistics of a small sample size. Figure 2b displays morphometric data for those 16 flank vents with HRSC DTM coverage. The relationships between the diameter, slope, height, and volume agree well with terrestrial small vents. The slope values were calculated using two methods. Method 1 used an equation that relates volume and area to slope from Hauber *et al.*, 2009 but assuming a conical shape. The slopes also represent the average slopes of the landforms and thus do not take into account steepening at the summit or burial of lower, more gently sloping portions of the landform. This method yielded average slope values slightly higher than those expected for low shields. Method 2 involved calculating average slopes of the vents using shapefiles and HRSC DTMs in JMars. This method yielded a lower average slope for each vent and a lower average slope for all 16 vents. Method 2 is likely more accurate in the case of this study, since many vents do not have an idealized conical shape and the volumes are not well constrained. These analyses suggest that these 16 features do represent small vents on Olympus Mons.

2.5. Flank Vent and Graben Spatial Density Calculations

We calculated the density of flank vents and graben as a function of distance from the actual geographic center of the volcano, rather than from the center of the offset summit caldera complex, to capture more area of the shield. In order to calculate the spatial density of vents and graben, we approximated Olympus Mons as a circle with a radius of 263 km, divided into six ring-shaped zones of equal area (~43,460 km²). This shape excluded most of the area of the flow aprons but incorporated the majority of the main shield. We then counted the number of vents and grabens within each ring of equal area and compared that value to the

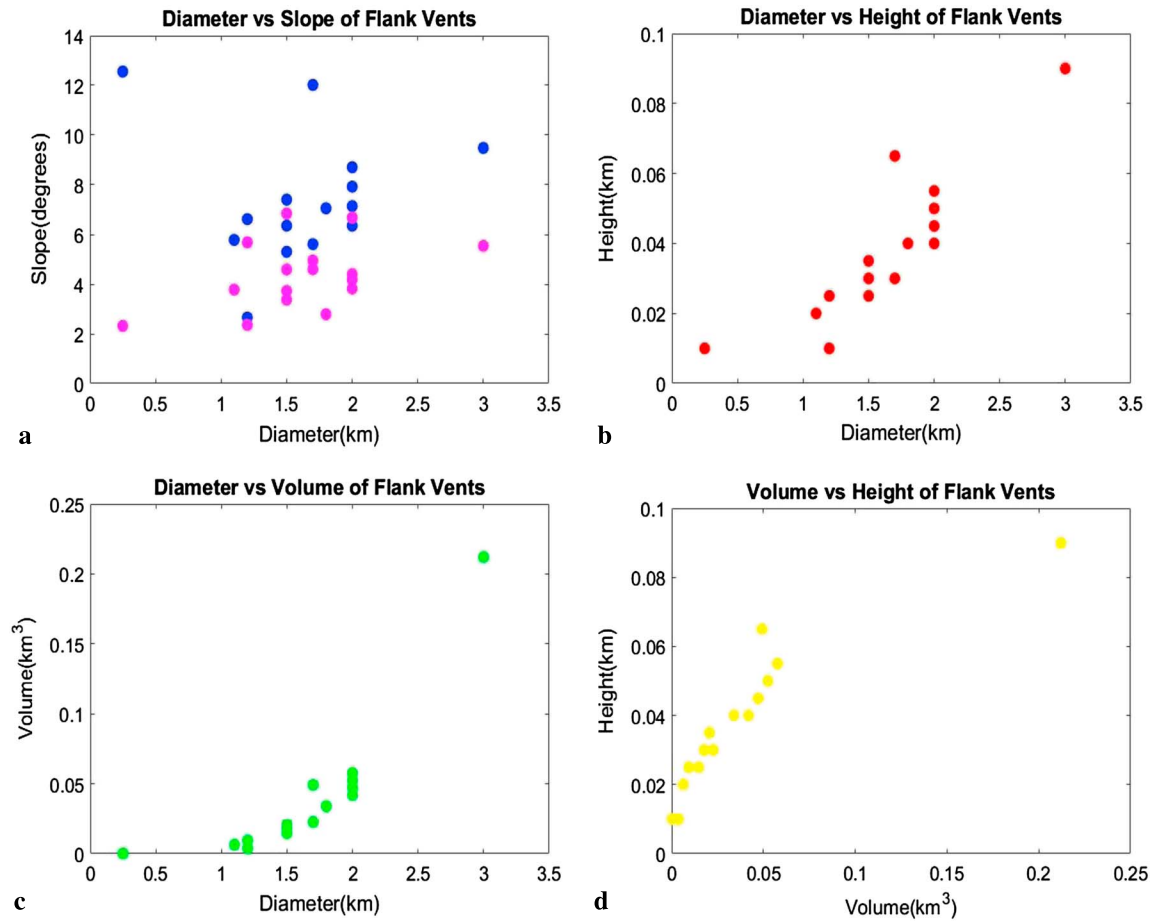


Figure 2. Morphometric relationships of flank vents ($n = 16$). (a) Magenta dots represent average slopes calculated using equation from *Hauber et al.* [2009]. Blue dots represent average slopes obtained using HRSC DTMs.

overall number of vents and grabens observed. This allowed us to see where vents and grabens were more concentrated on the shield relative to other areas.

2.6. Nearest Neighbor Analysis of Flank Vents

Nearest neighbor analysis provides a description of the degree of randomness of a population [*Clark and Evans, 1954; Bleacher et al., 2009*]. *Clark and Evans, 1954* used a ratio, R , to measure the degree to which a distribution departs from random with respect to the nearest neighbor. $R = 1$ indicates a random distribution, $R < 1$ indicates clustering, and $R > 1$ indicates dispersion. This technique has been applied to a variety of studies that characterize the evolution of small volcanic fields by determining the degree of clustering therein [*Bishop, 2008; Bleacher et al., 2009*]. If no clustering is found, and the volcanic field displays a random Poisson distribution, this suggests that the formation of each vent was unaffected by the formation of earlier vents. A non-random distribution suggests that the vents share the same source plumbing or branch of source plumbing.

3. Results

We identified 125 candidate flank vents and 84 grabens on Olympus Mons. In our survey, we included the northeast and southwest flow aprons as part of the Olympus Mons edifice. Due to uncertainty in the mode of formation of some features (e.g., those that might morphologically resemble flank vents but that were formed via other volcanic processes, such as lava fans that are built by flows emanating from lava tubes at slope breaks), we assigned to each a rating based on our confidence (i.e., likely, probably, unlikely, and very unlikely) that they are flank vents. If there was no observable relationship to other volcanic features, our confidence in a given landform being volcanic was increased. For example, a conical topographic high with

radially emanating flows was, we adjudged, a reasonable candidate for a low shield. If a feature occurred in close proximity to other features that offered an alternative mode of formation, our confidence in it being volcanic was decreased. For instance, ridges formed by lava tubes sometimes exhibit multiple points of lava effusion, which can look like primary vents [Bleacher *et al.*, 2007]. Features rated as unlikely or very unlikely to be vents are not included in the results we report here. The difference between landforms being rated as likely to be a vent versus probably being a vent was based on image quality (e.g., resolution, lighting, and dust opacity), whether HRSC DTM data were available and/or whether definitive morphological characteristics, such as flows emanating from a depression atop an isolated topographic high, were present. It is important to note that the exclusion from this paper of landforms to which we assigned an unlikely and very unlikely rating of being flank vents does not meaningfully change the results or implications of our study, because the spatial distribution and relative age of those ambiguous landforms are similar to those we consider likely and probable flank vents. Additionally, higher-resolution image and topographic data may help determine the nature of those equivocal landforms in the future. Here we report on 60 landforms we considered as likely or probable flank vents.

3.1. Flank Vents

Flank vents were identified primarily on the basis of their morphology. We considered positive-relief features with radiating lava flows emanating from a central crater or depression to be flank vents. Most of the flank vents sourced channelized flows, some of which appear to flow >15 km from the vent. On average, the flows originating at the flank vents are ~5 km in length. Bleacher *et al.* [2007] noted that some features previously identified as flank vents on Olympus Mons are in fact lava fans. From our survey, we also find that lava fans are a common landform on Olympus Mons. However, we are confident that the features we identified as vents are not lava fans but, instead, likely sites of magma eruption driven by subsurface transport via dike or sill propagation. It remains a challenging task to differentiate some features based solely on morphology, given the number of volcanic landforms with similar topographic expressions (such as lava fans versus low shields). Nonetheless, noting morphological and morphometric differences between these 60 landforms we identified as flank vents, we classified them into four categories (Figure 3): low shields ($n=43$), fissure vents ($n=7$), scoria cones ($n=6$), and lava lakes ($n=4$).

3.1.1. Low Shields

Of the 60 vents observed, we classified 43 as low shields (Figure 3b). Low shields are a common landform in the Tharsis province and occur in a variety of sizes [Wilson and Head, 1994; Bleacher *et al.*, 2009; Hauber *et al.*, 2009]. Low shields are positive topographic features with a convex profile and slopes averaging $\leq 1^\circ$ [Greeley, 1977; Greeley, 1982; Hauber *et al.*, 2009]. However, the summits of low shields can steepen to $\sim 5^\circ$. Slopes were calculated for 16 of the 43 low shields observed on Olympus Mons using two methods. Method 1, an empirical relationship, yielded an average slope for the 16 shields of $\sim 7^\circ$. Method 2, measured using the HRSC DTM, yielded an average slope for the 16 shields of $\sim 4^\circ$. We found Method 2 to be a more reliable measurement, given it comes directly from the data and does not rely on Method 1's assumptions of morphology. The low shields on Olympus Mons might be considered very low shields according to Hauber *et al.* [2009], since they have heights generally under 100 m. Based on the morphologies and morphometries we observed, we further divided the observed low shields into three types: Types 1–3 (Table 1). We interpret these types to represent a developmental sequence.

Type 1 low shields display radially emanating, tongue-shaped flows and are consistent with the previous definition, i.e., that they are positive-relief, convex landforms with low slopes [Greeley, 1977; Greeley, 1982] (Figure 4a). Type 1 accounts for 26 of the 43 low shields observed. The ratio of the width of the summit crater (W_{cr}) to shield diameter (W_{co}) has been used in studies of scoria cones, stratovolcanoes, and shields to distinguish between different types of volcanic constructs [Wood, 1979; Wood, 1980; Hauber *et al.*, 2009]. We applied this morphometric ratio to highlight the differences in shape between these shield types (Table 1). Type 1 low shields are on average ~700 m larger in width, but display a W_{cr}/W_{co} ratio (~ 0.06) between their Type 2 and Type 3 counterparts. This ratio is similar to the terrestrial average of ~ 0.08 but higher than the Martian average of ~ 0.031 [Wood, 1979; Hauber *et al.*, 2009]. Because of embayment relationships by later lavas, the diameters of these landforms we measured are apparent diameters and are thus minima values. Thus, the ratios in Table 1 are absolute maxima. Type 1 low shields display no obvious pattern to their distribution in regards to elevation or distance from the center of the volcano.

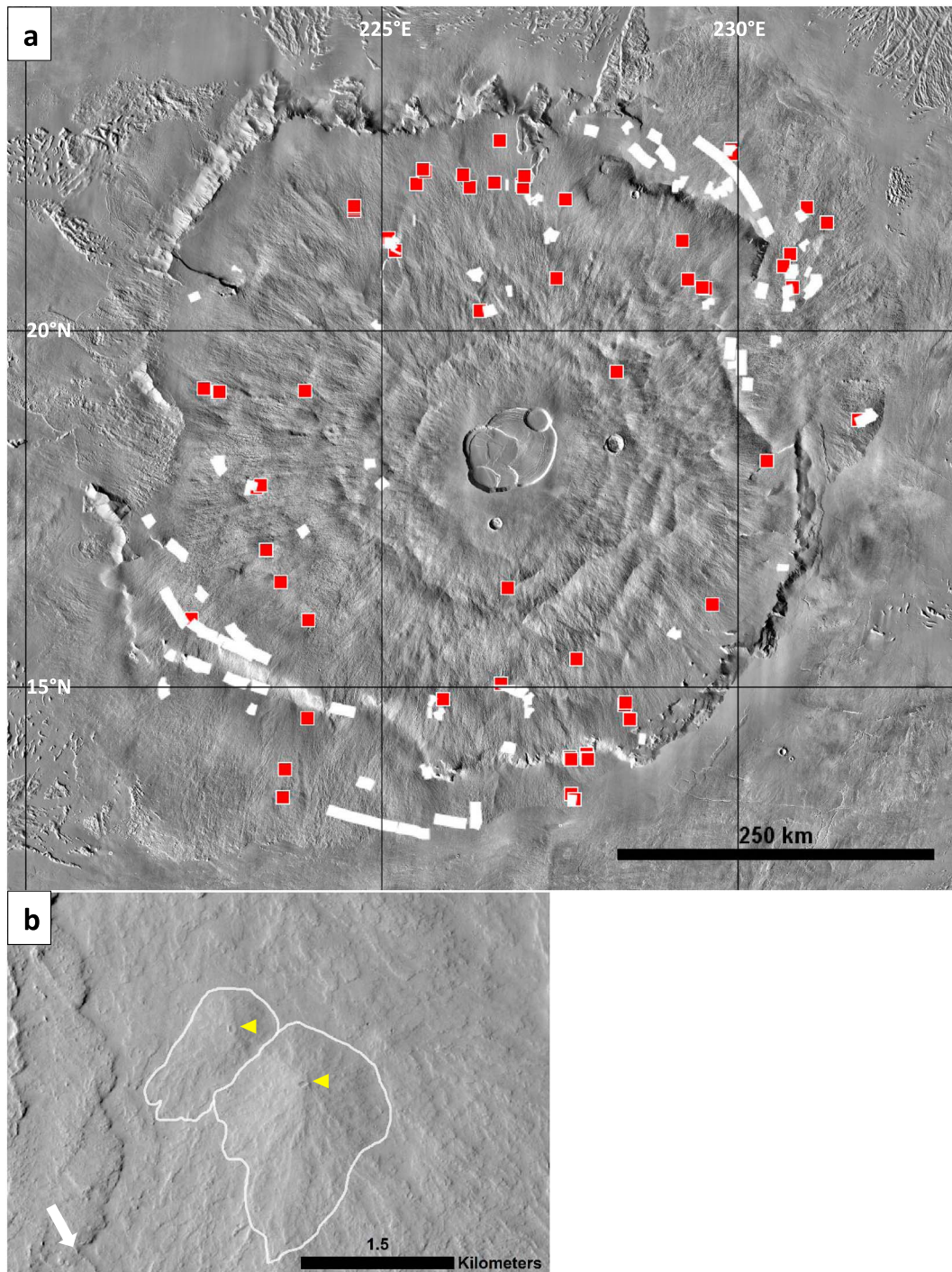


Figure 3. Mapped flank vents on Olympus Mons and examples of each type. Illumination is from the left in all images. White arrows mark the prevailing downslope direction. (a) THEMIS Day IR mosaic. Different color squares (yellow, white, green, and blue) denote Figures 3b–3e, respectively. CTX (b) P02_001920_1958_XN_15N132W, (c) P08_004109_2015_XI_21N134W, (d) P20_008684_2011_XN_21N129W, and (e) P21_009330_2008_XN_20N128W. (Figure 3a) Red squares mark location of vents. Note the occurrence of vents on the flow aprons and mantled portions of the escarpment. There is an apparent paucity of vents observed in the northwest. (Figure 3b) Example of two low shields observed along a flow-mantled portion of southern escarpment. These represent Type 1 low shields. White line represents the extent of shield visible. Yellow triangles point to summit craters. Image center located at 13.986°N, 227.896°E. (Figure 3c) Remnants of volcanic landform that interpreted as a scoria cone, although much of the edifice is embayed with lavas. Lava appears to have flowed into the summit crater. The mound to the east is interpreted as the remnants of another cone. Located at 21.286°N, 225.108°E. (Figure 3d) A fissure vent on the northeast flow apron. Note the raised edges of the fissure, indicating a possible spatter rampart. Located at 22.480°N, 229.935°E. (Figure 3e) A lava lake on the northeastern flow apron. Lava flows are outlined and appear to emanate from the lava lake and flow preferentially to the northeast. Located at 21.501°N, 231.254°E.

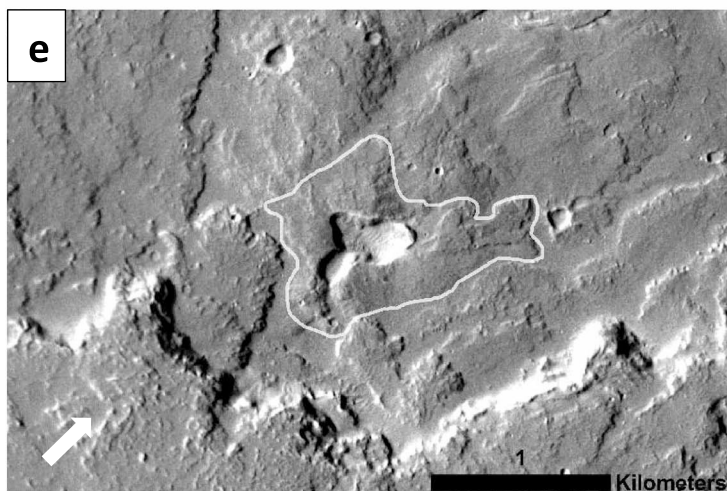
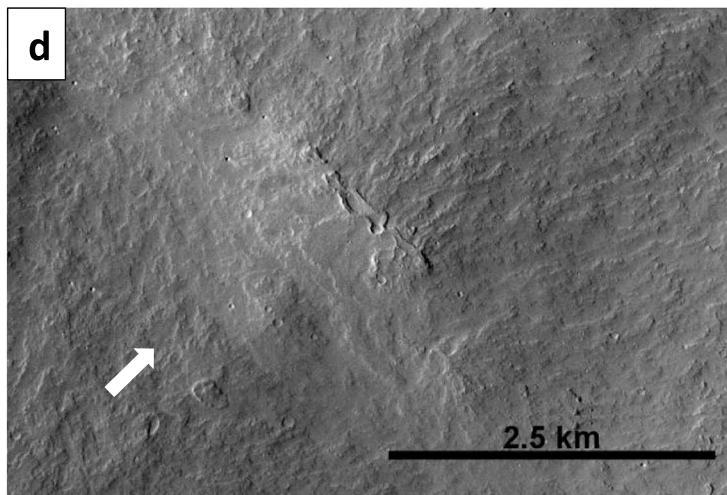
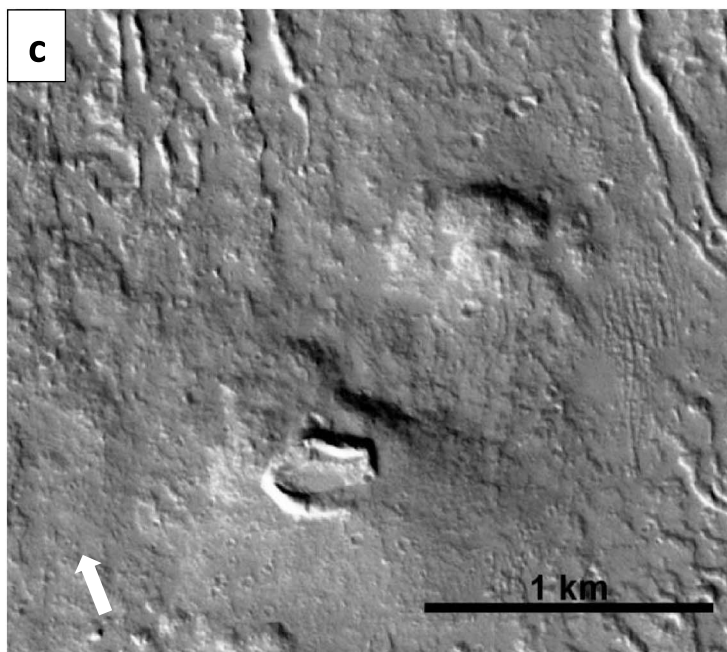


Figure 3. (continued)

Table 1. The Properties of Different Types of Low Shields Observed on Olympus Mons in This Study

Morphometric Properties of Low Shield Flank Vents			
	Type 1	Type 2	Type 3
Count	26	12	5
Average W_{cr} (km)	0.12	0.13	0.15
Average W_{co} (km)	1.7	1.0	1.6
W_{cr}/W_{co} ^a	0.06	0.13	0.05

^aRatio is the average of all the W_{cr}/W_{co} measurements taken not the average in the table. W_{cr} = crater width; W_{co} = cone width.

Type 2 low shields have the highest W_{cr}/W_{co} ratio (~0.13) of the three types and are built by several distinct, overlapping tabular flow lobes that give them a flower petal-like morphology (Figure 4b). The observed ratio is much higher than the terrestrial and Martian averages [Wood, 1979; Hauber *et al.*, 2009]. Although some portion of these shields might be buried beneath later, superposing

flows or obscured by dust, the crater-cone ratios are much higher than those measured for Type 1 shields, suggesting a possible difference in development of lava rheology. Indeed, the summit craters for Type 2 low shields are broader than Type 1 shields.

Type 3 low shields are defined by us as a combination between Types 1 and 2 low shields. These edifices display morphological elements of both other types. Usually, this combined morphology is manifest as a superposition relationship of Type 1 shield shape superposed on the flower petal morphology of Type 2 shields (Figure 4c). Most of the Type 3 landforms therefore appear to have developed first with the distinct, flat flow lobes of Type 2 shields and later transitioned to the narrower, tongue-shaped flows of Type 1 shields. The small number of Type 3 shields makes any statistical analysis of them less than robust. The W_{cr}/W_{co} ratio is similar to that of Type 1 low shields. This reflects the apparent tendency for the Type 1 shield morphology to overprint the earlier morphology of the Type 2 shield.

Under the assumption that each flow lobe reflects an eruptive event, we interpret Type 2 low shields as sites where lava erupted only a few times. Several of the Type 2 low shields occur in pairs or in threes, suggesting that they are sourced from the same branch of the Olympus Mons magma plumbing system. The larger summit craters and higher W_{cr}/W_{co} ratios of Type 2 low shields might suggest that these edifices represent a different type of constructional landform that deserves its own category. The presence of Type 3 low shields argues against this interpretation, however. Type 3 low shields may reflect the effects of changes in the style, frequency, and/or longevity of eruptions. Some Type 1 low shields could therefore start as Type 2 low shields, with that earlier phase being covered or buried by later flows. Thus, these different types of low shields may represent a developmental sequence, with Type 2 low shields representing the least evolved in this sequence and Type 1 low shields the most. The average volume of low shields on Olympus Mons volumes is ~0.03 km³. This value represents an underestimate due to the truncation of the true height and diameter of the feature by later flows that embayed the base of these landforms.

3.1.2. Cones

We identified six features we interpreted as scoria cones (Figure 3c) on the basis of morphology and morphometry (Table 2). They occur at various flank elevations and distances. All cones display embayment relationships with lava flows; some are almost completely buried. W_{cr}/W_{co} ratios for the cones (~0.15–0.4) agree well with Martian (~0.28) and terrestrial (~0.20–0.40) values for scoria cones [Wood, 1980; Hauber *et al.*, 2009; Brož and Hauber, 2012]. Once again, our values are overestimates because of the reduction in cone diameter by lava flow embayment. HRSC DTM coverage was available for only one cone, but its dimensions are near the resolution limit of the DTM [Jaumann *et al.*, 2007]. All of the landforms we identify as scoria cones appear degraded, and some exhibit asymmetries in plan view. Most are found near other volcanic landforms, such as low shields and fissure vents.

3.1.3. Fissure Vents

A small number of landforms we interpret as fissure vents ($n = 7$) were also observed (Figure 3d). Fissure vents are found at a variety of elevations and distances from the volcanic center. Most display a raised rim near the vent. Lava flows emanate from the vents. One fissure vent was imaged fully by an HRSC DTM on the lower flanks of Olympus Mons. Flows from this vent have constructed a low edifice ~100 m in height.

3.1.4. Lava Lakes

The landforms in this category ($n = 4$) are subcircular depressions that do not feature a distinct edifice, although flows emanate from them indicating that they were possible sources of effusive activity at some point (Figure 3e). We have interpreted these landforms as possible lava lakes. Most examples are filled

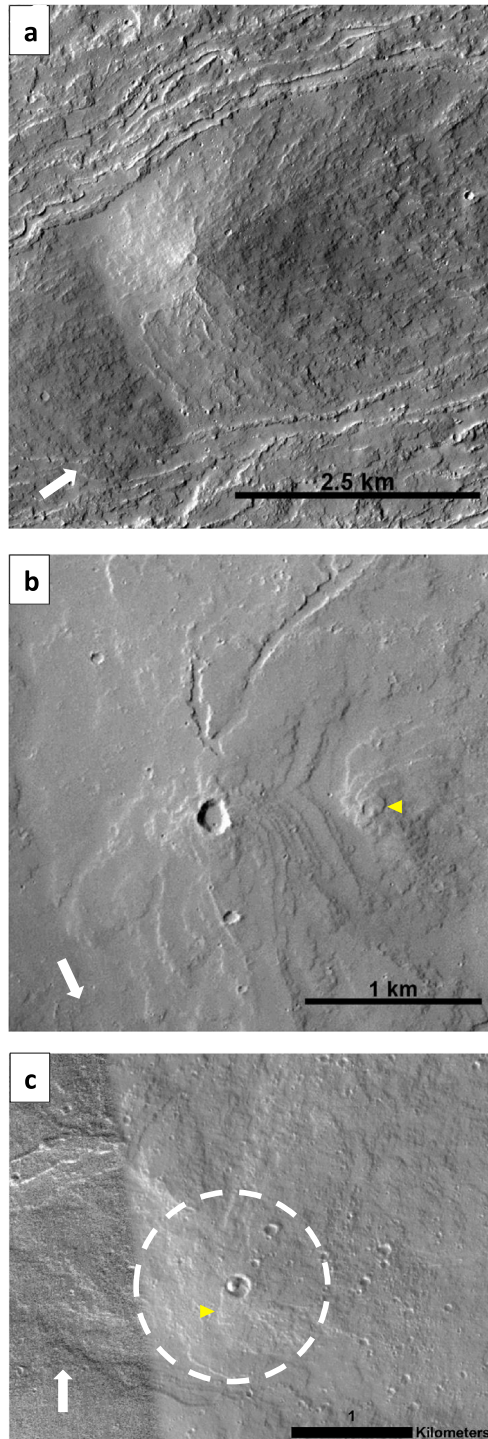


Figure 4. The three types of low shields observed on Olympus Mons. Illumination is approximately from the left in all images. White arrows mark the prevailing downslope direction. CTX (a) F23_044762_2008_XN_20N129W, (b) P21_009330_2008_XN_20N128W, and (c) P06_003265_2010_XN_21N133W. (Figure 4a) Example of a Type 1 low shield on eastern Olympus Mons. Lava flows and channels have diverted around the shield. Located at 20.604°N, 230.768°E. (Figure 4b) A Type 2 low shield. Note the flower petal morphology of the flow lobes on the flanks; these flows are flat and distinct. Yellow area points to a possible secondary vent located to the east. Lineaments to the north may represent fissures, lava channels, lava-rise pits, or grabens. Located at 18.744°N, 231.699°E. (Figure 4c) A Type 3 low shield. The white dashed circle denotes the approximate extent of the shield. Some flows exhibit flower petal morphology, whereas others do not. Yellow arrow points to particular flow displaying flower petal morphology. An anomalous dome structure is situated in the summit crater. Darker color on the left side of the image is an artifact. Located at 22.071°N, 226.584°E.

Table 2. W_{cr}/W_{co} Ratios for the Six Cones Observed in This Study^a
Morphometric Properties of Cones

	1	2	3	4	5	6
W_{cr}/W_{co}	0.240	0.150	0.400	0.250	0.286	0.280

^aCone 2 occurs along the mantled escarpment and has been modified by a channel flow that emerged from its summit.

with dust and aeolian bed forms. No correlation exists between this vent type and flank elevation or distance from the center of Olympus Mons. No spectrum of degradation was observed either. Generally, these features are a few hundred meters across.

3.1.5. Flank Vent Distribution

We measured the elevation of each vent above the surrounding plains and the lateral distance of each vent from the center of the volcanic caldera complex. This is slightly east of the geographic center of the volcano as a function of Olympus Mons's asymmetry relative to its caldera complex. The center of the nested caldera complex (approximately 18.33°N, 226.83°E) was chosen as the center here, because direct pathways to the magma chamber below are assumed [Wood, 1984; Zuber and Mouginis-Mark, 1992; Thomas et al., 1990]. As ~2 km of lava from Tharsis and the Tharsis Montes have embayed Olympus Mons to the east, all vent elevation values are referenced to the elevation of the plains west of Olympus Mons that sit at an elevation of -2.5 km.

We found a bimodal distribution in flank vent location as a function of elevation on the volcano (Figure 5a). Vents occur preferentially at elevations between 8 and 14 km and below 4 km. Flank vents are observed along portions of the escarpment that have been draped by lava flows to a smaller degree than observed in the northeast and southwest. Thus, vents at elevations lower than ~8 km are situated exclusively on either the flow aprons that drape the escarpment to the northeast and southwest or on portions of the scarp that have been mantled by lava flows. No vents are observed above elevations of 20 km. Above this point, the texture of terrain has been smoothed by volcanic activity from the summit calderas and possibly by the incorporation of dust and volatiles.

The location of flank vents as a function of distance from the center of the volcano follows the generally unimodal distribution shown in Figure 5b. It is important to note that the basal escarpment is situated an average of ~263 km from the center of the volcano (varying from ~225 km in the east to ~320 km in the northwest). Vents occurring farther than this average distance mostly occur on the flow aprons and portions of the escarpment mantled with lava flows. The lower flanks of Olympus Mons, below the flank terraces and above the escarpment, tend to have more gentle slopes than the rest of the volcano. Figure 6 shows that most of the flank vents occur in these areas of relatively more shallow slopes. Spatial density calculations of the flank vents reveal that ~78% ($n = 47$) of the flank vents occur inside the average distance to the escarpment (~263 km), with the remaining vents situated beyond the escarpment. Of those 47 flank vents, ~74% ($n = 35$) are located between 204 and 263 km from the center of the volcano. This shows that flank vents are more common on the lower flanks of Olympus Mons. Figure 7 depicts the azimuthal distribution of flank vents showing a tendency of vents to have formed in the north-northeast and southeast.

3.1.5.1. Nearest Neighbor Analysis

Studies of terrestrial volcanoes have shown that the spacing of vents can also be used as a proxy for source depth [Wood, 1980; Bleacher et al., 2009; Hauber et al., 2009]. We found that the flank vents on Olympus Mons display moderate clustering, with $R = 0.66$. Given that the vents occur on the flanks of a major shield volcano, this spatial relationship is expected and is consistent with the vents sharing a common source region. It is unclear whether vents identified on the flow aprons have the same source(s) as the vents on the main Olympus Mons shield, since numerous lava flows and other volcanic features seemingly unrelated to Olympus Mons are observed at the distal margins of the volcano [Sherwood et al., 2013; Chadwick et al., 2015]. However, nearest neighbor analysis and the other observations and measurements conducted in this study support these vents being sourced from Olympus Mons.

3.2. Graben

We identified 84 grabens on the flank of Olympus Mons (Figure 8). These are small-scale features, ranging 2–87 km in length and 100–2000 m in width (Figures 9a and 9b). The grabens' widths are scale invariant, with most grabens <300 m in width despite lengths of several to tens of kilometers. Many of the grabens are linear but concentric about the center of the volcano, whereas others are curved but are also concentric about the

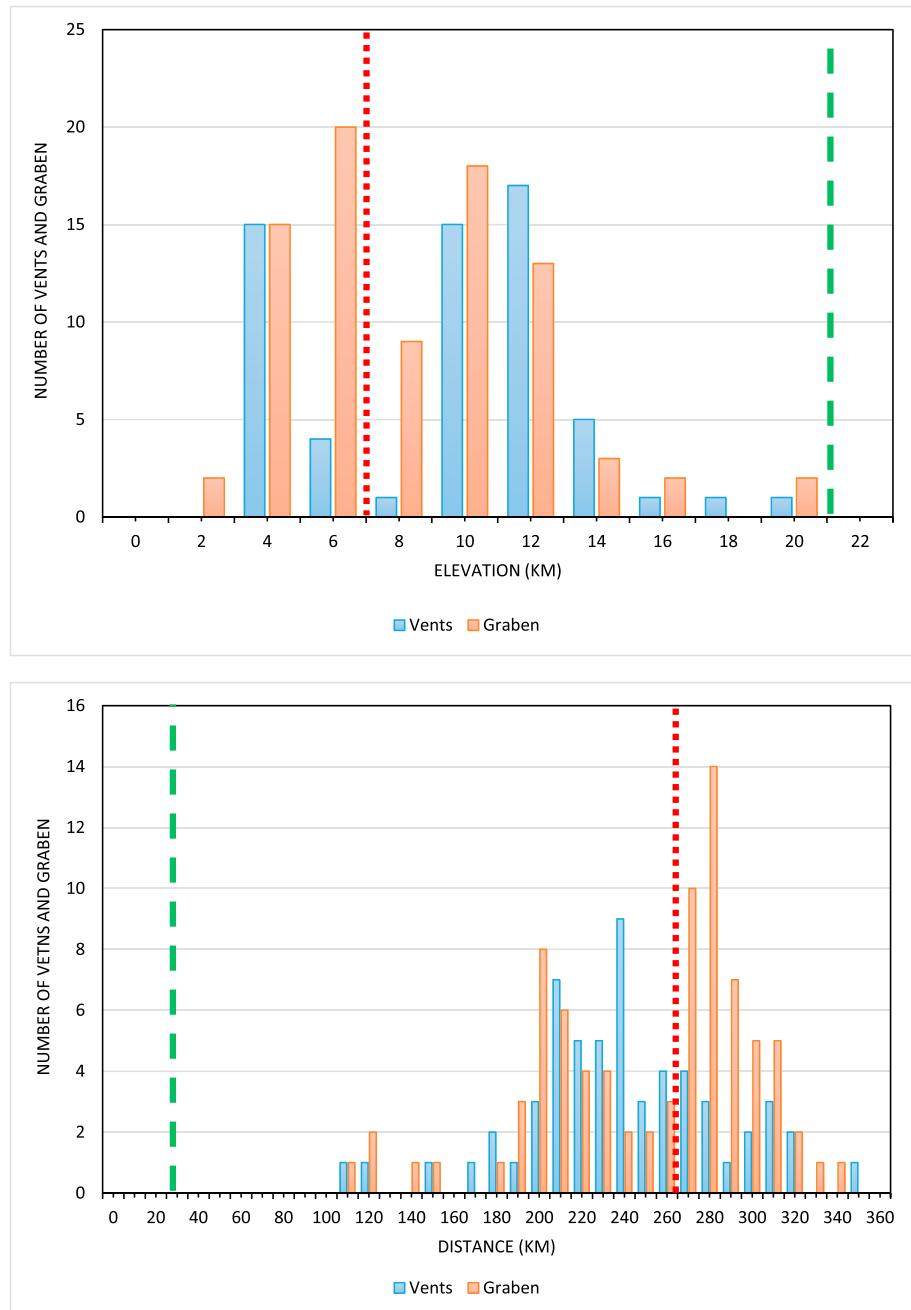


Figure 5. The distribution of flank vents and grabens as a function of elevation and distance from the center of the summit caldera complex of Olympus Mons. The red dotted line marks the average location of the escarpment. The dashed green line denotes the approximate edge of the summit caldera complex. (a) Number of flank vents and grabens as a function of elevation. The distribution of vents and grabens is fairly normal. The relative dearth of vents and grabens around 8 km reflects the lack of such landforms in association with the basal escarpment. (b) Number of flank vents and grabens as a function of distance from the summit. Grabens display a bimodal distribution as a function of distance from the center of Olympus Mons. The dip in the distribution corresponds to the escarpment. The distribution suggests that grabens are just as likely to form upslope as downslope of the scarp.

center of the volcano. The five widest grabens are observed on the volcano’s northeastern flow lobe. These wider grabens are similar in width to some of the grabens observed on the Tharsis Montes [Carr, 1974]. We included them in this study because they possess a similar spatial relationship and orientation as the smaller graben. Due to the small size of the graben we identified on the flanks, many were not resolvable with HRSC

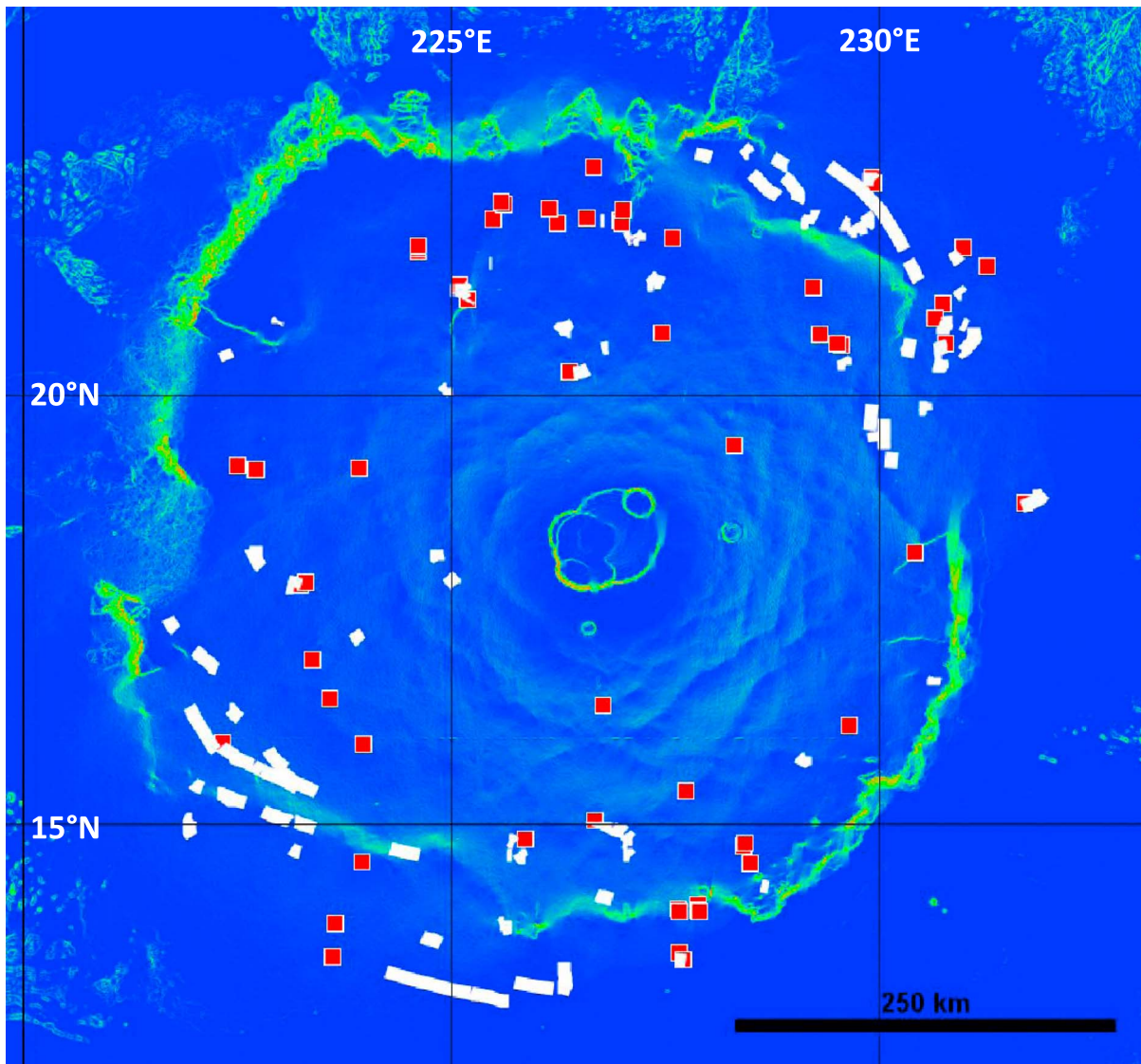


Figure 6. MOLA slope map with flank vents is denoted by red boxes and grabens denoted by blue lines. Red boxes and white lines have been enlarged for visibility. The majority of vents and grabens occur on shallower slopes. Few grabens occur at higher elevations.

DTMs or MOLA shots, consistent with widths generally <300 m (only a couple of pixels across). The depths of wider grabens >300 m were also not resolvable indicating that they are perhaps only tens of meters in depth. A HiRISE image confirms that these features are topographically subtle and that most display a muted appearance likely due to dust cover. Fifty-four ($\sim 64\%$) of the grabens we observed have experienced little or no modification by subsequent volcanism based on their relatively “fresh” appearance, crisp boundaries, and lack of lava flow superposition (Figure 9c). Six have been superposed by impact craters 0.2–0.5 km across. Three grabens crosscut either flank vents or flank vent derived flows (Figure 10). Two grabens on the southwestern flow apron display ambiguous spatial relationships to pit crater chains. Only one of the grabens display possible collocation with volcanic material, which may be emanating flows.

3.2.1. Graben Distribution

Grabens display a bimodal distribution with respect to elevation and distance from the center of the caldera, with most occurring at elevations of 2–12 km (Figure 5). This distribution indicates that grabens occur at similar distances away from the escarpment upslope and downslope. A number of grabens occur on the northeastern and southwestern flow aprons, which skew the results by increasing the average radial distance of graben from the summit. The paucity of grabens at radial distances of 240–270 km is probably due to the

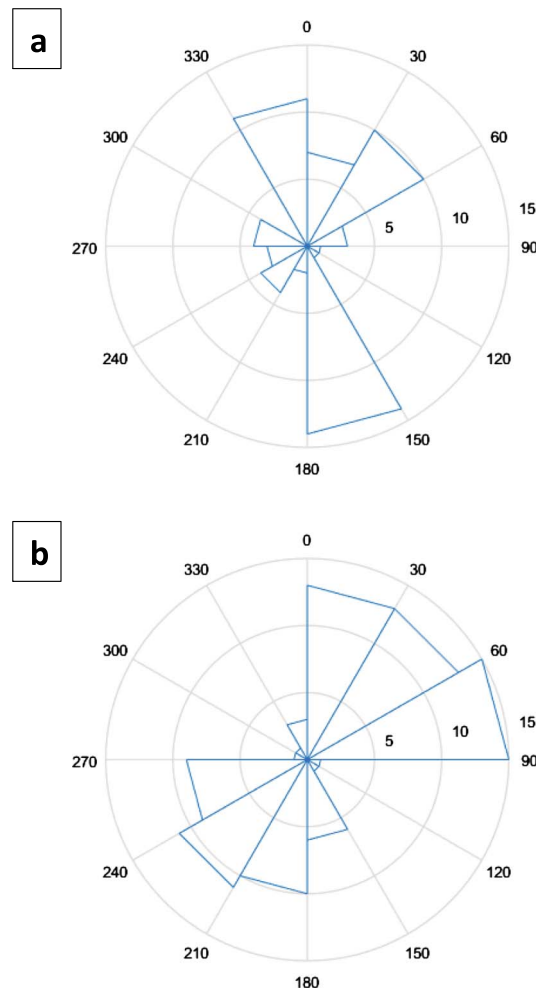


Figure 7. (a) The azimuthal distribution of flank vents relative to the geographic center of the volcano (18.39°N, 226.45°E). Vents are grouped into 30° bins. The length of bins reflects the number of elements in each bin (0–15). 0° is due north. Vents occurring to the northeast and southwest occur mostly on the flow aprons. The vents in the southeast generally occur on portions of the escarpment that have been mantled by lava flows, similar to the NE and SW. (b) The azimuthal distribution of grabens relative to the geographic center of Olympus Mons (18.39°N, 226.45°E). Grabens are grouped in 30° bins. The length of bins reflects the number of elements in each bin (0–15). 0° is due north. Note the paucity of grabens observed to the west-northwest and east-southeast. The distribution is skewed by the preferential occurrence of grabens on the northeast and southwest flow aprons.

these vents sourced channelized flows that traveled for several kilometers. Most of the flank vents on Olympus Mons are low shields. We classified these landforms into three types (i.e., Types 1–3) which may represent a developmental sequence in the formation of these landforms. The prevalence of low shields, but the paucity of other vent types, on the volcano offers an explanation in which two processes acted in concert: (1) the most recent lavas erupted on Olympus Mons had a low volatile content and/or low viscosity and (2) burial by lava flows preferentially obscured subtle topographic constructs, i.e., fissure vents and lava lakes, rather than low shields. In regards to fissure vents, the apparent dearth of this landform on Olympus Mons may be a function of their evolution into low shields. Alternatively, another possible reason is that fissure vents and lava lakes did not commonly form on Olympus Mons.

presence of the escarpment. Similar to flank vents, most of the grabens are situated on the shallower slopes of the lower flanks, although several occur on the terraced upper flanks (Figure 6) but none above 20 km. A density calculation similar to one for flank vents was performed for grabens. We found that 50% of the grabens are located within 263 km of the center of the summit caldera, producing a bimodal distribution. Figure 7b shows the azimuthal distribution relative to the geographic center of the volcano. The plot reflects the tendency of grabens to occur on the flow aprons and mantled portions of the escarpment. A similar observation was found on Ascræus Mons by *Byrne et al.* [2012], with grabens there occurring mostly off the main shield and on the lava aprons, instead.

4. Discussion

In this study, we have focused on the identification and characterization of previously unmapped features on Olympus Mons: flank vents and graben. Our observations suggest that small-scale, possibly dike-fed volcanism, and circumferential extension were active on Olympus Mons in the Late Amazonian (≤ 700 Ma) [*Neukum et al.*, 2004; *Werner*, 2009; *Tanaka et al.*, 2014]. We therefore interpret for Olympus Mons a history similar to that inferred for other large Martian shields, such as Ascræus Mons [*Bleacher et al.*, 2009; *Byrne et al.*, 2009; *Byrne et al.*, 2012]. Many of the features observed in this study represent processes that occurred relatively late in Martian geologic history [*Neukum et al.*, 2004; *Bleacher et al.*, 2007; *Werner*, 2009; *Tanaka et al.*, 2014]. This observation has broad implications for vent formation and evolution, surface deformation, subsurface magma propagation, and the development of shield volcanoes on Mars.

4.1. Flank Vents

Flank vents provide information on effusion rates, eruption style, and magma volatility. We observed at least 60 flank vents on Olympus Mons. Many of

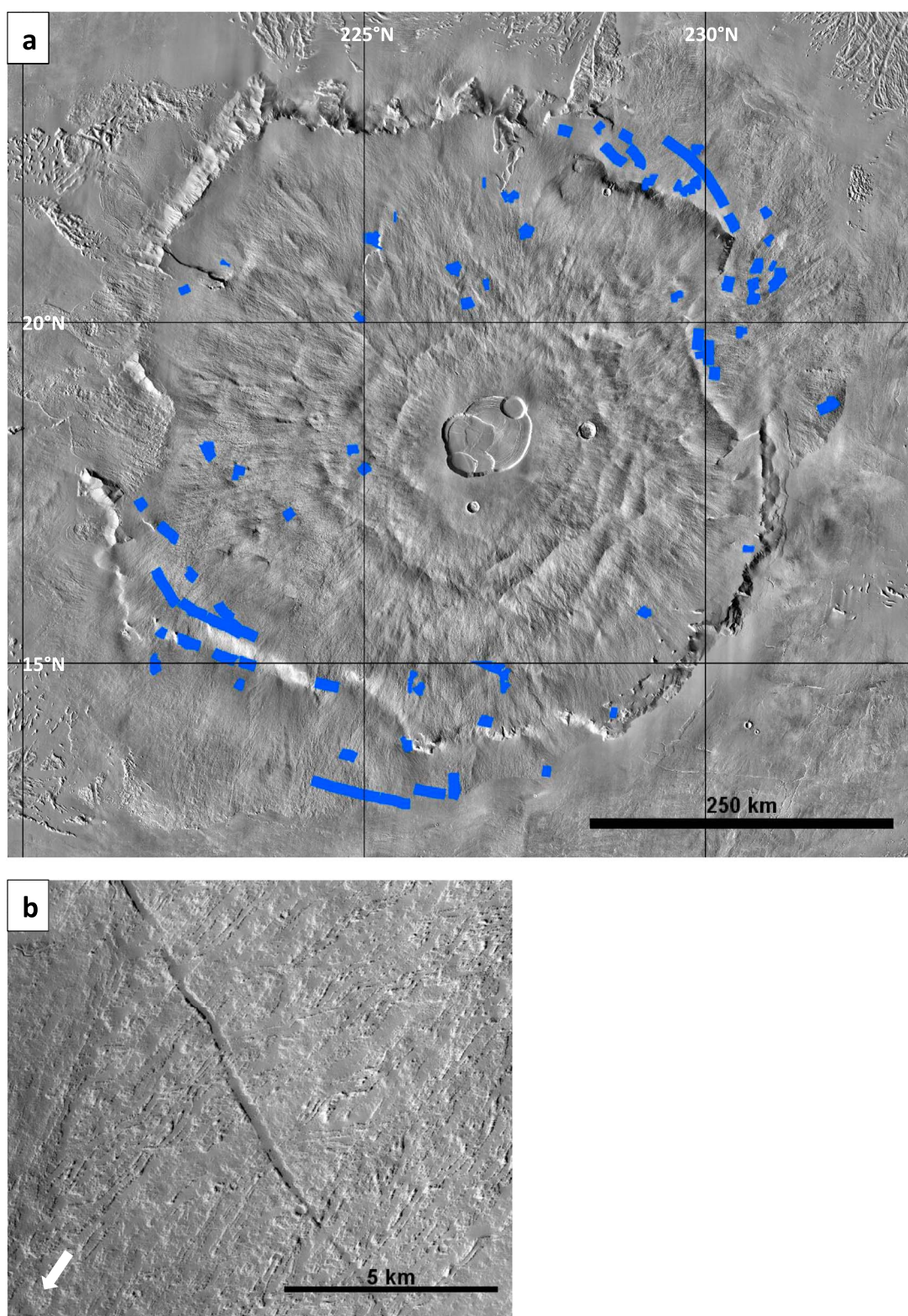


Figure 8. Mapped grabens on Olympus Mons. Illumination is from the left in both images. (a) Map of the 84 grabens we observed on Olympus Mons. THEMIS Day IR base map. Blue lines enlarged for visibility. (b) CTX image of a graben on the southwestern flow apron. Pictured graben is ~150 m wide. White arrow marks the prevailing downslope direction.

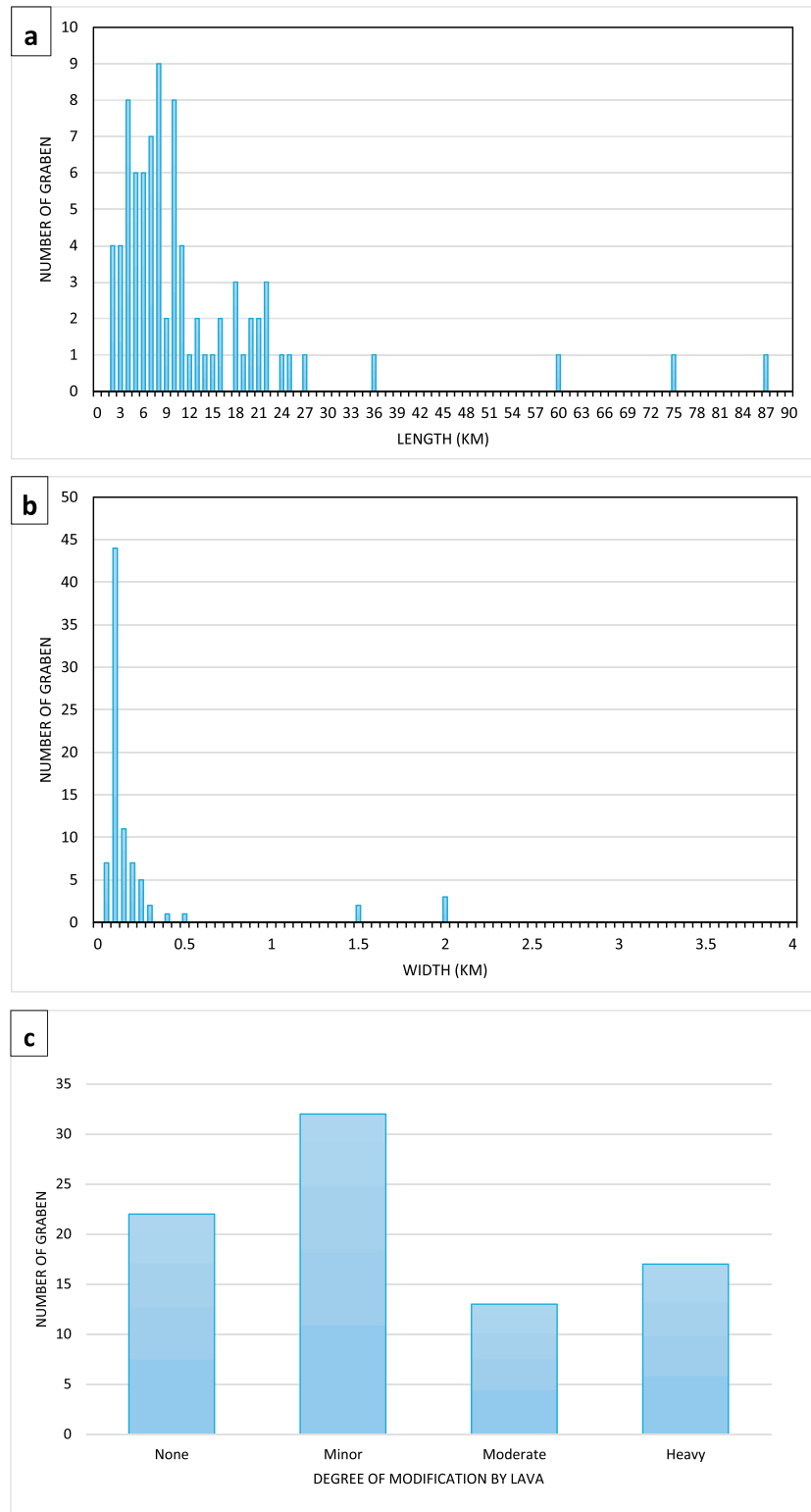


Figure 9. Length distribution, width distribution, and the degree of modification of grabens. (a) Length distribution reveals that grabens are generally < 30 km in length. (b) Width distribution of grabens reveals that grabens are generally < 0.5 km in width. (c) Assessment of the degree of modification by subsequent lava flows. Modification refers to how much of the graben’s length has been superposed by lava flows. None: no lava flows crosscut the length graben; minor: one lava flow has crosscut the graben; moderate: two lava flows have crosscut the graben; and heavy: three or more lava flows have crosscut the graben.

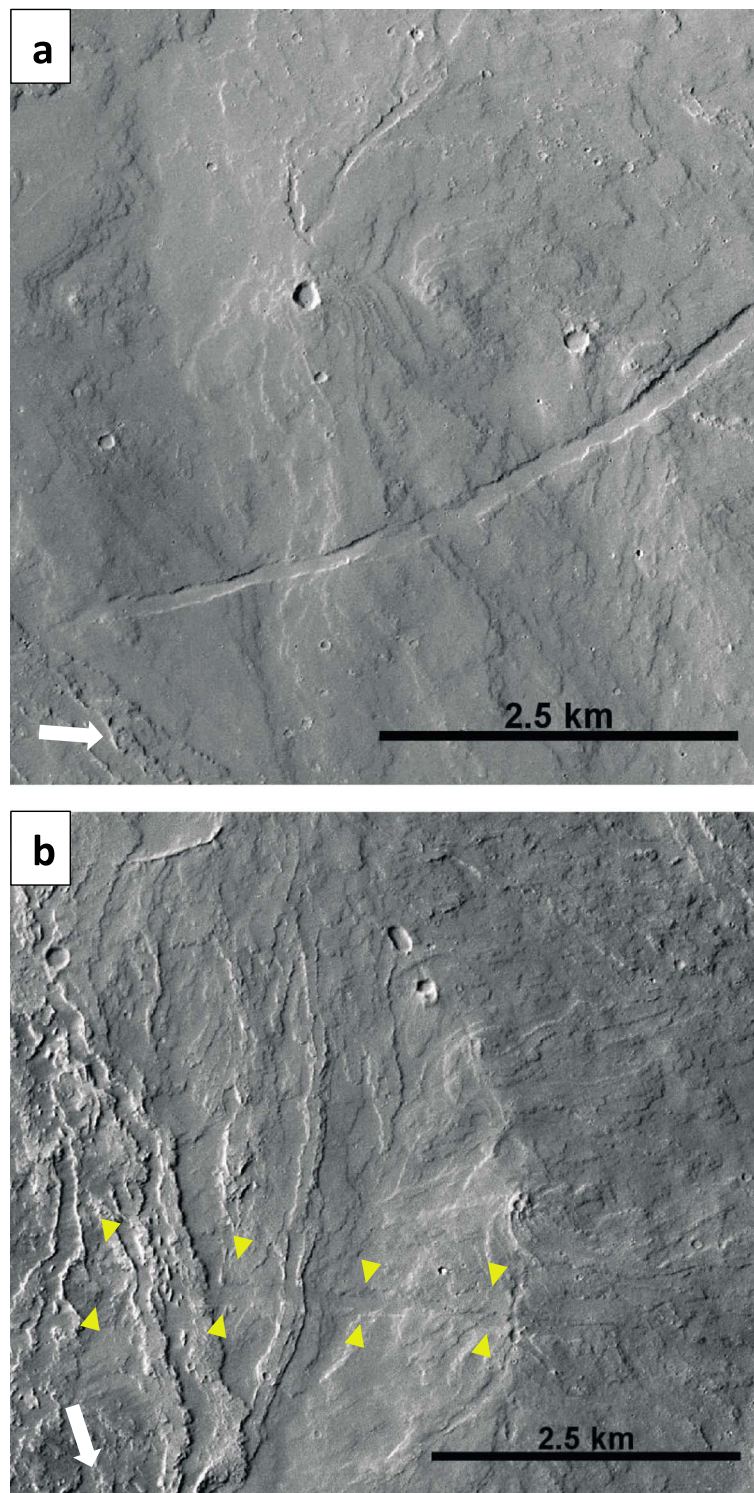


Figure 10. Two examples of grabens crosscutting flank vents or flank-vent-derived flows. CTX (a) P21_009330_2008_XN_20N128W and (b) B21_017888_1944_XN_14N132W. (Figure 10a) A Type 2 low shield located on the northeastern flow lobe. A graben has crosscut flows from the vent. Located at 18.745°N, 231.6978°E. (Figure 10b) A Type 2 low shield located on the southern, mantled length of the escarpment. Note the subtle topography of the graben in the lower image. Located at 13.421°N, 227.706°E. White arrows point in downslope direction. Yellow arrows indicate grabens, which are barely discernible on the landscape. Illumination is from the left.

The first process is supported by the presence of the ubiquitous lava tubes and channels observed on the flanks [Carr, 1973; Carr *et al.*, 1977; Bleacher *et al.*, 2007]. The surface flows of Olympus Mons have been dated as Late Amazonian, specifically 100–700 Ma [Neukum *et al.*, 2004; Werner, 2009; Tanaka *et al.*, 2014]. Smaller areas on the shield have been assigned even younger dates of ≤ 20 Ma, with some flows as young as 5 Ma [Neukum *et al.*, 2004; Werner, 2009]. The flank vents themselves are embayed by lava flows fed primarily by these lava tubes and channels [Bleacher *et al.*, 2007]. The prevalence of channel and tube-fed lava flows and the lack of small parasitic cones support the eruption of mostly low-volatile lavas in recent Martian geologic history. The lavas of Olympus Mons have constructed an edifice 22 km above the surrounding plains, which is indicative of very prolonged volcanic activity. It is plausible that many, if not most, flank vents that formed on the edifice have been buried, with those we observe today corresponding to the last episode of major shield volcanism.

The observation of scoria cones on Olympus Mons suggests that some of the lavas erupted onto the surface were relatively enriched in volatiles. Explosive basaltic volcanism is theorized to more readily occur on Mars than Earth because of lower atmospheric pressure [Wilson and Head, 1994]. That does not exclude the possibility of phreatomagmatic cones forming on Olympus Mons. Due to the height of Olympus Mons and other large Martian volcanoes, it has been hypothesized that ice may have accumulated on the middle to upper flanks as a result of snow fall and glaciation and may exist beneath a layer of dust and assorted volcanic deposits [Tanaka, 1985; Helgason, 1999; Neukum *et al.*, 2004; Bleacher *et al.*, 2007]. The lack of any observable and identifiable phreatomagmatic landforms or products suggests a lack of magma-water interactions during Late Amazonian resurfacing, which in turn indicates either a lack of ice during Late Amazonian resurfacing or little or no volcanic activity since the formation of interstitial ice. If the landforms we observe are in fact scoria cones, then given the ages found for the flanks of Olympus Mons in earlier studies, these small cones have survived for much longer periods of time than their terrestrial counterparts. This finding is consistent with terrestrial scoria cones having a lifespan of only a few million years, owing mostly to erosion [Hooper and Sheridan, 1998]; erosional processes are far slower on Mars, and so such small volcanoes on Olympus Mons may persist for tens or hundreds of millions of years. Scoria cones have been identified in a variety of locations across Mars, but attempts to determine that their ages are ongoing [Brož and Hauber, 2012]. For Olympus Mons, it is possible that the survival of cones against erosion for tens or hundreds of millions of years may be due in part to their partial burial by lava flows and dust mantle, which armored them. However, these processes also obscure the shape of the scoria cones making them harder to identify, with the end result being similar to the problem of cone loss through erosion on Earth.

The majority of flank vents are found on the shallower slopes of the lower flanks of the volcano. This spatial distribution suggests that favorable conditions for eruptions occurred away from the summit. Kervyn *et al.* [2009] postulated that such a distribution of vents may indicate magma pathways in the subsurface are compromised by the effect of flexure upon the volcano itself. The load of a volcano on the lithosphere can favor the development of vents near its base, because flexure and compression of the edifice itself precludes the ascent of magma to its summit [Kervyn *et al.*, 2009]. This explanation and the degree of clustering lends credence to the inference that the vents at the base of Olympus Mons are likely related to volcanism occurring on the edifice and that they may share a similar source or sources.

4.2. Graben

We observed 84 grabens on Olympus Mons. These grabens are largely concentric about the summit of the volcano, with some displaying an arcuate shape. The tendency for grabens to occur on the lower flanks of Olympus Mons suggests that extension occurred primarily on the lower flanks. The small size of the grabens, relative to their larger counterparts on other volcanoes in the Tharsis province, suggests a proportionally lower degree of extensional strain. The apparent lack of superposition by subsequent lava flows, dearth of overprinting by impact craters, and relative crispness of their boundaries imply that the grabens are relatively young and formed during waning volcanic activity. However, there is a possibility that the grabens' predate Late Amazonian volcanism and were simply reactivated and their expression reprinted onto the surface. Their formation may have occurred as a result of magma propagation via dikes or spreading of the volcano's lower flanks. Many grabens occur on the flow aprons to the northeast and southwest. Although grabens are found on portions of the escarpment mantled by cascading lava flows, unmantled portions of the escarpment do not host grabens. These fresher, and thus steeper, portions of the scarp may not thus display grabens because extensional stresses could be manifested as slumped blocks or relatively fast-acting mass wasting.

4.3. Relationship Between Flank Vents and Graben

The spatial relationship of flank vents to other features on Olympus Mons allows us to establish a time line for their development. Although most vents occur on the main shield, more than 20% occur on or below the escarpment. Vents along the escarpment are situated within sections that have been mantled by lava flows that were closely emplaced after the events that led to the formation of the scarp in the first place. This distribution suggests that the formation of flank vents was coeval with the volcanic activity responsible for mantling the escarpment. The aureole deposits encircling Olympus Mons, material thought to be derived from massive landslides originating from the base of the volcano, have been dated as Middle Amazonian [Tanaka, 1985; Mougini-Mark and Christensen, 2005; Tanaka et al., 2014]. The vents observed at or below the escarpment therefore formed after this time. Those vents located above the escarpment appear to have escaped burial by subsequent lavas, and so we can constrain the formation of these vents to a time of waning volcanic activity.

The present surface of Olympus Mons has been dated as Late Amazonian, which suggest the flank vents are at least similar in age [Neukum et al., 2004; Werner, 2009; Tanaka et al., 2014]. Although mantled in ~1 m of dust [Christensen, 1986], most of the vents observed display a paucity of impact craters hundreds of meters in size as well as crisp vent morphologies. Many lava flows appear to have been diverted around these vents, suggesting that these small volcanoes were constructed before or concurrent with the emplacement of the effusive flows (Figure 4a) [Bleacher et al., 2007]. These spatial relations indicate that the observed flank vents represent some of the last vestiges of Late Amazonian volcanic resurfacing of the shield.

The superposed grabens on the lower flank imply a geologically recent radial extensional stress field applied to the lower portion of the edifice [McGovern and Solomon, 1993; Byrne et al., 2012; Weller et al., 2014]. All observed grabens crosscut lava flows. Most grabens have experienced little or no modification by later lava flows via infill and overprinting. We cannot rule out the erasure of pre-Late Amazonian graben by later volcanic activity, whose bounding faults have not been reactivated.

In three observed cases, all on flow aprons or flow mantled escarpment, the grabens appear to cut flank vent constructs or flank-vent-derived flows. In these cases, the grabens are therefore younger than the flank vents. It is difficult to determine whether or not all the grabens are younger than the flank vents. The possibility must also be considered that the grabens predate the flank vents and later tectonic activity reactivated the graben-bounding faults, which would have reasserted the topographic expression of the grabens on the vent or vent-associate lava flows. The youngest flows on Olympus Mons are generally found on the lower flanks [Neukum et al., 2004; Werner, 2009; Tanaka et al., 2014]. The majority of grabens occur on the lower flanks of Olympus Mons and crosscut some of the youngest flows, which attests to their relatively young age. Grabens observed on segments of mantled escarpment indicate that some such structures formed or were reactivated following the mantling of the escarpment by lavas. A lack of graben on steeper segments of the escarpment not mantled by lava flows is consistent with a scenario under which the creation of the scarp erased any preexisting graben. Alternatively, the extensional stresses driving graben formation resulted in localized collapse and mass wasting on the steeper slopes rather than the formation of discrete, localized extensional structures. Taken together, these superposition relations suggest that grabens are among the youngest endogenic geological features on Olympus Mons.

4.4. Magma Plumbing System

The most recent activity within the Olympus Mons caldera complex has been dated to 100–200 Ma [Neukum et al., 2004; Werner, 2009; Tanaka et al., 2014]. These ages represent the time of the last subsidence of the magma chamber, which would correspond with the emplacement of the latest lavas on the caldera floors. Given that the bulk of the edifice is older than these relatively young ages [Isherwood et al., 2013], only the most recent volcanism on the flanks (e.g., those flows \leq 200 Ma) postdate the last instances of caldera collapse. Kervyn et al. [2009] suggested that a conduit plugged by solidified magma would lead to eruptions near the base of the volcano. The vents at lower flank elevations suggest a common source, either a primary or secondary magma source [Wood, 1980; Bleacher et al., 2009; Pozzobon et al., 2015]. The sheer size of Olympus Mons suggests that this hypothesis is tenable: the occurrence of flank vents indicates that in some cases dikes may have propagated hundreds of kilometers laterally [Mougini-Mark and Christensen, 2005;

Byrne *et al.*, 2012]. Numerical models predict that radial dike propagation would be favored assuming a concentric σ_3 extensional stress field [McGovern and Solomon, 1993]. Alternatively, the existence of multiple magma reservoirs within the edifice cannot be ruled out. A décollement, a plane of mechanical weakness between two rock masses, has been hypothesized to underlay Olympus Mons [Byrne *et al.*, 2013; Weller *et al.*, 2014]. Additionally, dike propagation, in conjunction with a detachment surface at depth, could also provide a mechanism for collapse of the volcano's base [Elsworth and Day, 1999; Helgason, 1999; Kervyn *et al.*, 2009]. As a result, the process responsible for flank volcanism may also have played a role in the formation of the escarpment, albeit earlier in Olympus Mons' history. Conversely, the extensional stresses on the lower flanks of Olympus Mons could have provided pathways for magma to reach the surface and promoted flank volcanism. It is likely a combination of these processes operated on the lower portion of Olympus Mons.

4.5. Late Amazonian Tectonism

Previous studies of the tectonics of the large Martian volcanoes have focused largely on the flank terraces [Carr, 1973; Thomas *et al.*, 1990; McGovern and Solomon, 1993; Byrne *et al.*, 2009; Byrne *et al.*, 2012]. These features are interpreted to be the surface expression of thrust faulting resulting from the volcano sagging into its underlying basement [McGovern and Solomon, 1993; Byrne *et al.*, 2009; Byrne *et al.*, 2012; Byrne *et al.*, 2013]. In contrast, grabens on the flanks of Olympus Mons are indicative of an extensional stress regime. This interpretation agrees with model predictions of gravity spreading [Tanaka, 1985; Thomas *et al.*, 1990; McGovern and Solomon, 1993; Byrne *et al.*, 2009] or possibly magma propagation via dike emplacement [Elsworth and Day, 1999; Kervyn *et al.*, 2009]. The processes of gravity spreading or dike emplacement are not mutually exclusive, however. The occurrence of flank vents supports the emplacement of dikes; however, observed compressional features off the main shield suggest that gravity spreading linked to the underlying décollement is plausible also [Weller *et al.*, 2014]. Superposition relationships suggest that such an extensional stress regime occurred during waning Late Amazonian volcanic activity. This observation is supported by the lack of substantial lava overprinting on the grabens, and presence of graben on some vent constructs. The maximum ages of the grabens are established by the youngest ages of the surfaces they crosscut. Some grabens may be very young, especially those observed on the southwest flow apron, where flows are dated at ≤ 20 Ma [Neukum *et al.*, 2004]. The lack of lava flow superposition of many grabens suggests they were created, or their expression reasserted by fault reactivation, during waning volcanic activity. The extensional stress field that produced the grabens therefore must have been present in the Late Amazonian [Neukum *et al.*, 2004; Werner, 2009; Tanaka *et al.*, 2014]. Byrne *et al.* [2012] proposed that the arcuate grabens around Ascræus Mons might have been formed earlier in the volcano's evolution, buried by subsequent volcanism and then reactivated by subsequent downflexing of new shield material. The concentric and arcuate grabens observed around Ascræus Mons occur not only on the shield but also in the surrounding volcanic plains. Although no concentric or arcuate grabens are observed in the young plains immediately surrounding Olympus Mons, some exist farther away but display ambiguous relationships with Alba Mons [Isherwood *et al.*, 2013]. The lack of observed grabens in the plains surrounding Olympus Mons does not preclude the possibility of the grabens observed on Olympus Mons representing reactivation of earlier tectonism. Alternatively, grabens formed in the plains surrounding Olympus Mons may have since been buried and not since reactivated. Other studies have identified recent instability within the basal escarpment in the form of flank collapse driven by radially directed extension, specifically on the eastern scarp, which is supported by volcano-concentric shortening features in the plains surrounding Olympus Mons [Weller *et al.*, 2014]. The graben suggests that extensional deformation has occurred on Olympus Mons since the Late Amazonian, and an extensional stress field may be currently acting on the lower flanks of Olympus Mons today.

4.6. Development of Martian Shields

The developmental sequence of Olympus Mons appears similar to that proposed by Byrne *et al.* [2012] for Ascræus Mons and possibly the other Tharsis Montes. Olympus Mons underwent an initial shield building stage that began in the Late Noachian or Early Hesperian (~ 3.6 Ga) [Werner, 2009; Tanaka *et al.*, 2014]. Like Ascræus Mons, Olympus Mons was primarily built by effusive tube-fed and channelized lava flows [Carr, 1973; Carr *et al.*, 1977; Wilson and Head, 2002; Bleacher *et al.*, 2007; Byrne *et al.*, 2012]; construction of the volcano also likely featured a major intrusive component [Chadwick *et al.*, 2015]. Once the edifice reached some threshold height, possibly higher than its current elevation, it underwent gravitational deformation. This may have happened multiple times in its history. This gravitational deformation led to a combination of sagging

and spreading of the edifice, causing compression of the upper and middle flanks and producing thrust faults and the observed flank terraces there [Byrne *et al.*, 2009].

The growth of the shield produced extensional stresses on the lower flanks and combined with dike propagation and the likely presence of a basal décollement [e.g., Byrne *et al.*, 2013; Weller *et al.*, 2014] led to several episodes of large-scale sector collapse, most recently in the Middle to Late Amazonian, forming the circumferential escarpment and aureole deposits. Afterward, there was widespread resurfacing of the volcano via primarily effusive volcanic eruptions [Bleacher *et al.*, 2007; Chadwick *et al.*, 2015; Isherwood *et al.*, 2013]. This resurfacing created the large flow aprons to the northeast and southwest, similar to the large aprons observed on the Tharsis Montes. The presence of flank vents and graben on Olympus Mons is consistent with these landforms as being characteristic features of large Martian shields.

The construction of flank vents on Olympus Mons was spatially and volumetrically limited. Explosive eruptions on Martian shields played a small role during Late Amazonian resurfacing, suggesting some combination of volatile-poor magmas, slow ascent rates of magma in recent Martian history, and little interaction with near-surface ice. On Olympus Mons, concentric grabens developed concurrently with Late Amazonian resurfacing, indicative of an extensional stress field. Grabens continued to develop as the volcanic activity waned.

5. Conclusion

Through the identification, mapping, and characterization of flank vents and graben on Olympus Mons, we can constrain the volcanic and tectonic activity occurring on Olympus Mons in the Late Amazonian and further understand the development of large Martian shield volcanoes.

1. Small-scale, possibly dike-fed, volcanism and circumferential extension were active processes on Olympus Mons.
2. Flank vent construction on the midlower flanks of Olympus Mons suggests that conditions most favorable for dike propagation and eruptions were present here in the Late Amazonian. This favorability for eruptions on the lower flanks was likely tied to extension and preferential magma pathways caused by gravitational spreading of the volcano's lower flanks as the entire volcano downflexed its basement.
3. Flank vents exhibit morphologies and morphometries similar to their terrestrial counterparts. Some such landforms, termed here low shields, appear to display an evolutionary sequence in which they are built from a few, larger eruptions at first to many, smaller eruptions as they grow.
4. The observation of a small number of scoria cones on Olympus Mons indicates instances of explosive basaltic eruptions, albeit at very low volumes relative to the effusive activity that built the bulk of the edifice. The dearth of phreatomagmatic constructs on the volcano suggests a lack of magma-water interactions during the Late Amazonian.
5. Flank vents along the volcano's basal escarpment were likely formed by the volcanic activity responsible for emplacing the escarpment-mantling flows.
6. Given the sustained eruptions that produced the Olympus Mons volcano, it is plausible that earlier populations of flank vents that contributed to the construction of the edifice have been buried. The vents we observe today likely represent simply the last episode of vent construction.
7. The presence of graben, largely concentric, on the lower flanks of Olympus Mons suggests radial extension in the Late Amazonian. This extension either created the graben or reactivated faults from earlier grabens.
8. The small size (i.e., in terms of width, depth, and length) of these grabens relative to grabens on other Tharsis volcanoes suggests that the deformation was localized to the lower flanks of Olympus Mons.
9. The occurrence of grabens on the flow aprons and lava-mantled segments of the escarpment also suggests that, whatever their causal process, it operated primarily on the lower flanks. This is consistent with earlier findings for the volcano, in which upper and middle flanks experienced volcano sagging, placing that portion of the shield into compression, whereas the lower reaches of the volcano entered a state of net extension facilitated by volcano spreading along a basal décollement [Byrne *et al.*, 2013]. Spreading along the basal décollement and dike emplacement are likely culprits in the formation of the grabens.
10. Given existing measurements that suggest volcanism in the last 5–200 Myr in the areas where vents and grabens are found, these landforms may be some of the most recent volcanic and tectonic landforms documented on Mars.

Present-day Olympus Mons is a product of ~3.6 Ga of volcanic activity. The observation of flank vents and grabens on the volcano and their relationship to other volcanic and tectonic features there have enabled us to reconstruct a developmental sequence for Olympus Mons similar to that proposed for other volcanoes, e.g., Ascraeus Mons [Byrne *et al.*, 2013], with emphasis on the Late Amazonian. After construction of the bulk of the edifice, a combination of volcano sagging and spreading resulted in terracing of the upper flanks and in the formation of the basal escarpment and deposition of the aureoles. Subsequent volcanic resurfacing lasting through the Late Amazonian mantled the escarpment and produced flank vents on the main shield. This volcanic activity represented renewed growth of the shield, producing two lobes we have interpreted as aprons similar to those observed on the Tharsis Montes. As volcanism waned in the Late Amazonian, grabens formed in response to extension on the lower portion of the shield. In general, the grabens crosscut the escarpment and younger lava flows. Our interpretation agrees well with the development of other large shields on Mars, suggesting similar geologic processes operate for all large shield volcanoes on that world.

Acknowledgments

This work was supported by a NASA/JPL THEMIS contract 1228404. We very much appreciate the reviewers for very constructive feedback in helping improve this manuscript. We thank Jacob Bleacher and Paul K. Byrne for helpful in-person discussions. We would also like to thank Jacob Richardson for introduction to the Catalogue of Tharsis Small Volcanic Vents (<http://astrogeology.usgs.gov/search/details/Mars/Research/Volcanic/TharsisVents/>). In addition, we would like to especially thank Amanda Clarke and Kelin Whipple for improvements to earlier versions of this manuscript. NASA spacecraft data used in this study are referred to in section 5 of this paper. Data were obtained through Java Mission planning and Analysis for Remote Sensing (JMARS) software. Data used in the figures can be found in a supporting Excel file.

References

- Bishop, M. A. (2008), Higher-order neighbor analysis of the Tartarus Colles cone groups, Mars: The application of geographical indices to the understanding of cone pattern evolution, *Icarus*, *197*, 73–83, doi:10.1016/j.icarus.2008.04.003.
- Blasius, K. R., and J. A. Cutts (1981), Topography of Martian central volcanoes, *Icarus*, *45*, 87–112.
- Bleacher, J. E., R. Greeley, D. A. Williams, S. C. Werner, E. Hauber, and G. Neukum (2007), Olympus Mons, Mars: Inferred changes in late Amazonian aged effusive activity from lava flow mapping of Mars Express High Resolution Stereo data, *J. Geophys. Res.*, *112*, E04003, doi:10.1029/2006JE002826.
- Bleacher, J. E., L. S. Glaze, R. Greeley, E. Hauber, S. M. Baloga, S. E. H. Sakimoto, D. A. Williams, and T. D. Glotch (2009), Spatial and alignment analyses for a field of small volcanic vents south of Pavonis Mons and implications for the Tharsis province, Mars, *J. Volcanol. Geotherm. Res.*, *185*, 96–102, doi:10.1016/j.volgeores.2009.04.008.
- Bleacher, J. E., J. A. Richardson, P. W. Richardson, L. S. Glaze, S. M. Baloga, R. Greeley, E. Hauber, and R. J. Lillis (2010), Updates to the catalog of Tharsis province small volcanic vents, Mars, *Lunar Planet. Sci.*, *XLI*, Abstract 1615.
- Brož, P., and E. Hauber (2012), A unique volcanic field in Tharsis, Mars: Pyroclastic cones as evidence for explosive eruptions, *Icarus*, *218*, 88–99, doi:10.1016/j.icarus.2011.11.030.
- Byrne, P. K., B. van Wyk de Vries, J. B. Murray, and V. R. Troll (2009), The geometry of volcano flank terraces on Mars, *Earth Planet. Sci. Lett.*, *281*, 1–13, doi:10.1016/j.espl.2009.01.043.
- Byrne, P. K., B. van Wyk de Vries, J. B. Murray, and V. R. Troll (2012), A volcanotectonic survey of Ascraeus Mons, Mars, *J. Geophys. Res.*, *117*, E01004, doi:10.1029/2011JE003825.
- Byrne, P. K., E. P. Holohan, M. Kervyn, B. van Wyk de Vries, V. R. Troll, and J. B. Murray (2013), A sagging-spreading continuum of large volcano structure, *Geology*, *41*, 339–342, doi:10.1130/G33990.
- Carr, M. H. (1973), Volcanism on Mars, *J. Geophys. Res.*, *78*, 4049–4062, doi:10.1029/JB078i020p04049.
- Carr, M. H. (1974), Tectonism and volcanism of the Tharsis region of Mars, *J. Geophys. Res.*, *79*(26), 3942–3949, doi:10.1029/JB079i026p03943.
- Carr, M. H., R. Greeley, K. R. Blasius, J. E. Guest, and J. B. Murray (1977), Some Martian volcanic features as viewed from the Viking Orbiters, *J. Geophys. Res.*, *82*, 3985–4015, doi:10.1029/JA082i028p03985.
- Chadwick, J., P. McGovern, M. Simpson, and A. Reeves (2015), Late Amazonian subsidence and magmatism of Olympus Mons, Mars, *J. Geophys. Res. Planets*, *120*, 1585–1595.
- Christensen, P. R. (1986), Regional Dust Deposits on Mars: Physical Properties, Age, and History, *J. Geophys. Res.*, *91*(B3), 3533–3545, doi:10.1029/JB091iB03p03533.
- Christensen, P. R., et al. (2004), The Thermal Emission Imaging System (THEMIS) for the Mars 2001 Odyssey Mission, *Space Sci. Rev.*, *110*, 85–130.
- Clark, P. J., and F. C. Evans (1954), Distance to the nearest neighbor as a measure of spatial relationships in populations, *Ecology*, *35*(4), 445–453.
- Corrazato, C., and A. Tibaldi (2006), Fracture control on type, morphology and distribution of parasitic volcanic cones: An example from Mt. Etna, Italy, *J. Volcanol. Geotherm. Res.*, *158*, 177–194, doi:10.1016/j.volgeores.2006.04.018.
- Davidson, J., and S. DeSilva (2000), Composite volcanoes, in *Encyclopedia of Volcanoes*, edited by H. Sigurdsson, pp. 663–681, Academic Press, San Diego, Calif.
- Elsworth, D., and S. J. Day (1999), Flank collapse triggered by intrusion: The Canarian and Cape Verde archipelagoes, *J. Volcanol. Geotherm. Res.*, *94*, 323–340.
- Greeley, R. (1977), Basaltic “plains” volcanism, in *Volcanism of the Eastern Snake River Plain, Idaho: A Comparative Planetary Geology Guidebook*, edited by R. Greeley and J. S. King, pp. 24–44, NASA, Washington, D. C.
- Greeley, R. (1982), The Snake River Plain, Idaho: Representative of a new category of volcanism, *J. Geophys. Res.*, *87*, 2705–2712, doi:10.1029/JB087iB04p02705.
- Greeley, R., and P. D. Spudis (1981), Volcanism on Mars, *Rev. Geophys. Space Phys.*, *19*, 13–41.
- Hauber, E., J. Bleacher, K. Gwinner, D. Williams, and R. Greeley (2009), The topography and morphology of low shields and associated landforms of plains volcanism in the Tharsis region of Mars, *J. Volcanol. Geotherm. Res.*, *185*, 69–95, doi:10.1016/j.volgeores.2009.04.015.
- Helgason, J. (1999), Formation of Olympus Mons and the aureole escarpment problem on Mars, *Geology*, *27*(3), 231–234.
- Hooper, D. M., and M. F. Sheridan (1998), Computer-simulation models of scoria cone degradation, *J. Volcanol. Geotherm. Res.*, *83*, 241–267.
- Hulme, G. (1976), The determination of the rheological properties and effusion rate of an Olympus Mons lava, *Icarus*, *27*, 207–213.
- Isherwood, R. J., L. M. Jozwiak, J. C. Jansen, and J. C. Andrews-Hanna (2013), The volcanic history of Olympus Mons from paleo-topography and flexural modeling, *Earth Planet. Sci. Lett.*, *363*, 88–96.
- Jaumann, R., et al. (2007), The high-resolution stereo camera (HRSC) experiment on Mars Express: Instrument aspects and experiment conduct from interplanetary cruise through the nominal mission, *Planet. Space Sci.*, *55*, 928–952.

- Kervyn, M., G. G. J. Ernst, B. van Wyk de Vries, L. Mathieu, and P. Jacobs (2009), Volcano load control on dyke propagation and vent distribution: Insights from analogue modeling, *J. Geophys. Res.*, *114*, B03401, doi:10.1029/2008JB005653.
- King, J. S., and J. R. Riehle (1974), A proposed origin of the Olympus Mons escarpment, *Icarus*, *23*, 300–317.
- Malin, M. C., et al. (2007), Context camera investigation on board the Mars Reconnaissance Orbiter, *J. Geophys. Res.*, *112*, E05504, doi:10.1029/2006JE002808.
- McEwan, A. S., et al. (2007), Mars Reconnaissance Orbiter's High Resolution Imaging Science Experiment (HiRISE), *J. Geophys. Res.*, *112*, E05502, doi:10.1029/2005JE002605.
- McGovern, P. J., and S. C. Solomon (1993), State of stress, faulting, and eruption characteristics of large volcanoes on Mars, *J. Geophys. Res.*, *98*(E12), 23,553–23,579, doi:10.1029/93JE03093.
- McGovern, P. J., J. R. Smith, J. K. Morgan, and M. H. Bulmer (2004), Olympus Mons aureole deposits: New evidence for a flank failure origin, *J. Geophys. Res.*, *109*, E08008, doi:10.1029/2004JE002258.
- Mouginis-Mark, P. J., and P. R. Christensen (2005), New observations of volcanic features on Mars from the THEMIS instrument, *J. Geophys. Res.*, *110*, E08007, doi:10.1029/2009JE00241.
- Mouginis-Mark, P. J., and S. K. Rowland (2001), The geomorphology of planetary calderas, *Geomorphology*, *37*, 201–223.
- Nakamura, K. (1977), Volcanoes as possible indicators of tectonic stress orientation—Principle and proposal, *J. Volcanol. Geotherm. Res.*, *2*, 1–16.
- Neukum, G., et al. (2004), Recent and episodic volcanic and glacial activity on Mars revealed by the High Resolution Stereo Camera, *Nature*, *432*, 971–979.
- Plescia, J. B. (2004), Morphometric properties of Martian volcanoes, *J. Geophys. Res.*, *109*, E03003, doi:10.1029/2002JE002031.
- Pozzobon, R., F. Mazzarini, M. Massironi, and L. Marinangeli (2015), Self-similar clustering distribution of structural features on Ascraeus Mons (Mars): Implications for magma chamber depth, *Geol. Soc. London Spec. Publ.*, *401*, 203–218.
- Rowland, S. K. (1996), Slopes, lava flow volumes, and vent distributions on Volcán Fernandina, Galápagos Islands, *J. Geophys. Res.*, *101*(B12), 27,657–27,672, doi:10.1029/96JB02649.
- Tanaka, K. L. (1985), Ice-lubricated gravity spreading of the Olympus Mons aureole deposits, *Icarus*, *62*, 191–206.
- Tanaka, K. L., J. A. Skinner Jr., J. M. Dohm, R. P. Irwin III, E. J. Kolb, C. M. Fortezzo, T. Platz, G. G. Michael, and T. M. Hare (2014), *Geologic Map of Mars*, United States Geological Survey, Sci. Inv. Map 3392, Denver, Colo.
- Thomas, P. J., S. W. Squyres, and M. H. Carr (1990), Flank tectonics of Martian volcanoes, *J. Geophys. Res.*, *95*(14), 345–14,355.
- Weller, M. B., P. J. McGovern, T. Fournier, and J. K. Morgan (2014), Eastern Olympus Mons basal scarp: Structural and mechanical evidence for large scale slope instability, *J. Geophys. Res. Planets*, *119*, 1089–1109, doi:10.1002/2013JE004524.
- Werner, S. C. (2009), The global martian volcanic evolutionary history, *Icarus*, *201*, 44–68, doi:10.1016/j.icarus.2008.12.019.
- Wilson, L., and J. W. Head III (1994), Mars: Review and analysis of volcanic eruption theory and relationships to observed landforms, *Rev. Geophys.*, *32*(3), 221–263, doi:10.1029/94RG01113.
- Wilson, L., and J. W. Head III (2002), Tharsis-radial graben systems as the surface manifestation of plume-related dike intrusion complexes: Models and implications, *J. Geophys. Res.*, *107*(E8), 5057, doi:10.1029/2001JE001593.
- Wood, C. A. (1979), Monogenetic volcanoes of the terrestrial planets, in *Proceedings of Lunar Planetary Science Conference*, vol. 10, pp. 2815–2840, Lunar and Planetary Science Institute, Houston, Tex.
- Wood, C. A. (1980), Morphometric evolution of cinder cones, *J. Volcanol. Geotherm. Res.*, *7*, 387–413.
- Wood, C. A. (1984), Calderas: A planetary perspective, *J. Geophys. Res.*, *89*, 8391–8406, doi:10.1029/JB089iB10p08391.
- Zuber, M. T., and P. J. Mouginis-Mark (1992), Caldera subsidence and magma chamber depth of the Olympus Mons volcano, Mars, *J. Geophys. Res.*, *97*(E11), 18,295–18,307, doi:10.1029/92JE01770.
- Zuber, M. T., D. E. Smith, S. C. Solomon, D. O. Muhleman, J. W. Head, J. B. Garvin, J. B. Abshire, and J. L. Bufton (1992), The Mars observer laser altimeter investigation, *J. Geophys. Res.*, *97*, 7781–7797, doi:10.1029/92JE00341.